

Gaussian excitations model for glass-former dynamics and thermodynamicsDmitry V. Matyushov^{a)}*Department of Chemistry and Biochemistry and Department of Physics, Arizona State University,
P.O. Box 871604, Tempe, Arizona 85287-1604*C. Austen Angell^{b)}*Department of Chemistry and Biochemistry, Arizona State University, P.O. Box 871604,
Tempe, Arizona 85287-1604*

(Received 21 November 2006; accepted 11 January 2007; published online 6 March 2007)

We describe a model for the thermodynamics and dynamics of glass-forming liquids in terms of excitations from an ideal glass state to a Gaussian manifold of configurationally excited states. The quantitative fit of this three parameter model to the experimental data on excess entropy and heat capacity shows that “fragile” behavior, indicated by a sharply rising excess heat capacity as the glass transition is approached from above, occurs in anticipation of a first-order transition—usually hidden below the glass transition—to a “strong” liquid state of low excess entropy. The distinction between fragile and strong behavior of glass formers is traced back to an order of magnitude difference in the Gaussian width of their excitation energies. Simple relations connect the excess heat capacity to the Gaussian width parameter, and the liquid-liquid transition temperature, and strong, testable, predictions concerning the distinct properties of energy landscape for fragile liquids are made. The dynamic model relates relaxation to a hierarchical sequence of excitation events each involving the probability of accumulating sufficient kinetic energy on a separate excitable unit. Super-Arrhenius behavior of the relaxation rates, and the known correlation of kinetic with thermodynamic fragility, both follow from the way the rugged landscape induces fluctuations in the partitioning of energy between vibrational and configurational manifolds. A relation is derived in which the configurational heat capacity, rather than the configurational entropy of the Adam–Gibbs equation, controls the temperature dependence of the relaxation times, and this gives a comparable account of the experimental observations without postulating a divergent length scale. The familiar coincidence of zero mobility and Kauzmann temperatures is obtained as an approximate extrapolation of the theoretical equations. The comparison of the fits to excess thermodynamic properties of laboratory glass formers, and to configurational thermodynamics from simulations, reveals that the major portion of the excitation entropy responsible for fragile behavior resides in the low-frequency vibrational density of states. The thermodynamic transition predicted for fragile liquids emerges from beneath the glass transition in case of laboratory water and the unusual heat capacity behavior observed for this much studied liquid can be closely reproduced by the model.

© 2007 American Institute of Physics. [DOI: 10.1063/1.2538712]

I. INTRODUCTION

Viscous liquids close to the glass transition are usually characterized by a broad distributions of (their) relaxation times (stretched exponential kinetics) and stronger than Arrhenius (super-Arrhenius) dependence of the relaxation times on temperature.^{1,2} The stretched exponential kinetics is often represented by Kohlrausch–Williams–Watts (KWW) relaxation function

$$\phi^{\text{KWW}}(t) = \exp[-(t/\tau)^\beta], \quad (1)$$

where $\beta \leq 1$ is a stretching exponent and $\phi^{\text{KWW}}(t)$ is a normalized function representing some relaxing property. The temperature dependence of the relaxation time τ in this equation has been given many forms,³ but is most commonly

represented by the empirical Vogel–Fulcher–Tammann (VFT) law

$$\ln(\tau/\tau_0) = DT_0/(T - T_0), \quad (2)$$

were τ_0 is a characteristic time for liquid quasilattice vibrations. According to this equation, the relaxation time diverges at the VFT temperature T_0 below the glass transition temperature T_g ; T_0 is close to T_g for fragile liquids with super-Arrhenius kinetics and tends to zero for strong liquids with nearly Arrhenius relaxation.

At sufficiently low temperature, below the range of temperatures described by the mode-coupling theory,⁴ a liquid can be characterized by a set of minima (inherent structures) of the potential energy landscape divided by Stillinger into “basins of attraction.”⁵ The relaxation then occurs by a sequence of activated transitions⁶ between basins or collections of basins separated by low barriers (metabasins).^{7–9} While opinions of its origin differ, there is much evidence for a dynamic crossover temperature in fragile liquids, usually

^{a)}Electronic mail: dmitrym@asu.edu^{b)}Electronic mail: caangell@asu.edu

corresponding to the critical temperature of mode coupling theory, where relaxation times are about 10^{-7} s.¹⁰ Phenomenological theories, usually operating below this critical temperature, differ in their attribution of the driving force responsible for activated events.

The Adam–Gibbs theory¹¹ suggests that entropy controls the activation process. According to this line of thought,^{12–14} the divergence of the relaxation time at T_0 is caused by a decrease of the number of available states related to the configurational entropy $S_c(T)$. The relaxation time is given by the Adam–Gibbs relation

$$\ln(t/\tau_0) = \frac{\Delta}{TS_c(T)}, \quad (3)$$

which anticipates a growing length-scale ξ attributed to cooperatively rearranging regions. ξ diverges as $S_c(T)^{-1/3}$ on approach to the Kauzmann temperature T_K at which the configurational entropy vanishes^{11,15,16}

$$S_c(T_K) = 0. \quad (4)$$

The free-volume theory^{17,18} also considers entropy as the driving force for the glass transition in terms of the volume available for reorganizing the liquid. This “free” volume becomes increasingly scarce on cooling, eventually leading to a divergent relaxation time at the VFT temperature. The analysis of T , P viscosity data, however, indicates that it is temperature and not density that is the primary factor behind the super-Arrhenius kinetics.¹⁹

The coefficient Δ in Eq. (3) can be related to system properties within the concept of entropic droplet.^{20–22} Following arguments by Lubchenko and Wolynes²³ and by Bouchaud and Biroli,²⁴ the probability of creation of a droplet of size ξ is a competition of the surface, $\propto \xi^2$, and entropic bulk, $\propto \xi^3$, effects

$$P(\xi) \propto \exp[-\sigma(\xi)\xi^2 + S_c\xi^3]. \quad (5)$$

The probability minimizes at the stationary point of the exponent. Scaling of the surface tension with the droplet size of the form $\sigma(\xi) \propto \xi^{-1/2}$ results in the Adam–Gibbs law for the relaxation time, which, in this concept, corresponds to the time of creating a mobile region rich in configurational entropy. This picture, however, does not directly address the question of the origin of viscous flow,⁶ assuming that the mosaic structure of the dynamically exchanging mobile and immobile regions will have all the properties necessary to facilitate shear relaxation. The divergent length scale of mosaic regions scales as²⁵ $\xi \propto S_c(T)^{-2/3}$ in contrast to $\xi \propto S_c(T)^{-1/3}$ scaling for the length of cooperative regions in the Adam–Gibbs theory.

The Adam–Gibbs relation can be tested by calorimetry^{26,27} or by using relaxation times and configurational entropies from computer experiments.^{28–34} In the former case, one has to assume that S_c can be approximated by the excess entropy of a liquid over the crystal S^{ex} , although this is known to be a poor approximation in many cases.^{35–39} Nevertheless, the Adam–Gibbs equation is known to work well for both S^{ex} and S_c , although it does not produce perfectly straight lines for $\ln(\tau)$ vs $1/TS^{\text{ex}}$, in particular for fragile liquids. The use of S^{ex} in the Adam–Gibbs equa-

tion generally fails above the temperature T_B at which the dynamics change character (e.g., bifurcation into α and β processes).²⁷ The Adam–Gibbs equation with S^{ex} used for S_c is often equivalent to the VFT equation because many glass formers^{27,40} empirically follow the $1/T$ entropy decay

$$S^{\text{ex}}(T) = S_0(1 - T_K^{\text{exp}}/T), \quad (6)$$

where T_K^{exp} is what we will call the experimental Kauzmann temperature obtained by extrapolating $S^{\text{ex}}(T)$ to zero, in contrast to the thermodynamic Kauzmann temperature T_K defined by Eq. (4). Equation (6) often applies to configurational entropies obtained from simulations, although bilinear in $1/T$ forms have also been used to fit the data.^{41,42}

A strong experimental argument in favor of the Adams–Gibbs picture is the near equality⁴³ of the Kauzmann temperature T_K^{exp} and the VFT temperature T_0 . Further evidence is provided by the good account it gives of the pressure dependence of the glass transition temperature.^{44–46} However, the theoretical relevance of the concept of nucleation of cooperatively rearranging regions is not clear. Given the fact that laboratory glass formers and model fluids equilibrated at higher temperatures in computer experiment approximately follow Eq. (6), one wonders to what extent the combination of Eqs. (3) and (6) is just a successful mathematical relation, reproducing the VFT law in Eq. (2), and whether activated events in supercooled liquids are really driven by the entropy. The resolution of this problem is important from a general perspective since the Adam–Gibbs picture puts supercooled liquids in a unique position within the more general problem of activated events in condensed matter. For most cases, including the vast majority of chemical reactions, excess kinetic energy at a transforming unit or a molecular mode, and not the entropy, is the driving force which lifts the system to the top of the activation barrier. This, more traditional, view of relaxation of supercooled liquids is advocated by models that consider kinetic energy or enthalpy as the driving force of activated transitions.⁴⁷

In models of activation controlled by the kinetic energy, one considers excitations to a common high-energy level above the “top” of the landscape corresponding to high-temperature diffusion.⁴⁸ The energy of the starting point at a basin minimum is treated as a random variable within trap models^{9,49} or random-walk models.^{50–52} All such models result in activated kinetics with a temperature-dependent activation energy. However, since the probability of transition is finite at each temperature, no divergent relaxation time appears in these models.

A potential advantage of the energy models is the opportunity to unite the thermodynamics and dynamics of supercooled liquids within one conceptual framework and this is the motivation of the present paper. In the past, the two-state model by Angell and Rao⁵³ led to configurational entropies that are in quite good agreement with experimental data.⁵⁴ The model suggests that the thermodynamics of supercooled liquids can be described by an ensemble of noninteracting two-state excitations,⁵⁵ each creating an excess of entropy.⁵⁶ A recent extension of the model⁵⁷ considered two Gaussian manifolds of levels (2G model) instead of two discrete states of the original two-state model. This variant of the random

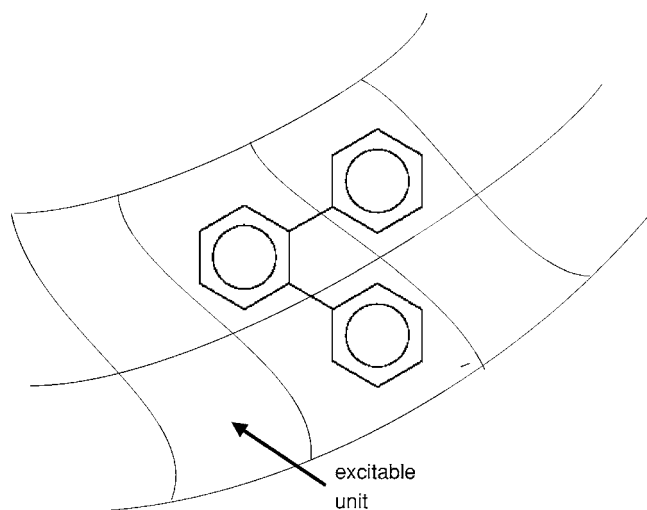


FIG. 1. Excitable units of a glass former in real space.

energy model, conceptually related to Bässler's random-walk picture,^{50,51} allowed an accurate fit of the laboratory and simulation data for heat capacities and configurational entropies. Here, we present a somewhat simplified version of this model that considers excitations from the single-energy level of the ideal glass to a Gaussian manifold of configurationally excited states (1G model). The thermodynamic analysis is then further used as a basis for a dynamic model of configurational excitations.

Our model of dynamics of viscous liquids follows the philosophy of the energy models of activation in that it considers the probability of accumulating kinetic energy sufficient to lift a "structural element" (or "excitable unit," see Fig. 1) to an energy level corresponding to the activated state of the high-temperature relaxation. The kinetic energy supplied by the surroundings of a given excitable unit is a fluctuating variable with a fluctuation width related to the ruggedness of the landscape through the configurational heat capacity. The average of the fluctuations of the kinetic energy results in a relation for the relaxation time which gives an increase of the activation energy with decreasing temperature in terms of the configurational heat capacity, rather than the configurational entropy of the Adam-Gibbs theory. The new relation gives an account of experimental dielectric relaxation comparable to the Adam-Gibbs formula, but more acceptable in several ways to be discussed later.

II. THERMODYNAMICS OF CONFIGURATIONAL EXCITATIONS

A. Formulation of the model

We conceive an excitation^{53,54,57} to be a local increase in potential energy that results from a collisional redistribution of kinetic energy among some minimum group of "rearrangeable units" of the liquid structure. In this redistribution a "unit" (Fig. 1) that undergoes an excessively anharmonic vibrational displacement can get trapped by the motions of neighbors that act to prevent a return of the unit to its original center of oscillation, such that some kinetic energy will be lost from the vibrational manifold and stored in the con-

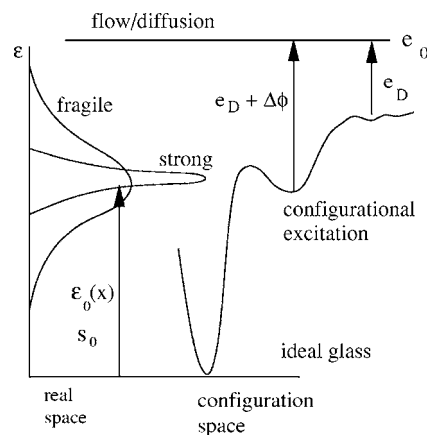


FIG. 2. Configurational excitations and flow/relaxation events in the 1G model. The thermodynamics of supercooled liquids is represented in real space by excitations from a single energy level of the ideal glass into a Gaussian manifold of configurationally excited states. Each excitation lifts the energy of an excitable unit (Fig. 1) by energy $\epsilon_0(x)$ [Eq. (22)] and entropy s_0 . The distribution of these states is much broader for fragile liquids than for intermediate and strong liquids. Relaxation is described by the dynamics of activated transitions in configuration space from basin minima of configurationally excited states to a common energy level e_0 above the top of the energy landscape. The activation barrier $e_D + \Delta\phi$ is a sum of the high-temperature activation energy e_D and the drop $\Delta\phi$ of the average energy of the basin minima from the high-temperature plateau.

figurational manifold. It is the constant and repeated exchange of energy between these manifolds that is the essence of configurational equilibration. The ability to store potential energy by this mechanism determines the configurational heat capacity.

The mathematical realization of this concept assumes that a liquid can be divided in real space into excitable units that follow the statistics of independent entities. Since these units form a continuous dense liquid phase and should be interacting, their actual interactions are represented by mean-field parameters of excitation energy ϵ_0 , excess entropy s_0 , and excess volume v_0 . Each excitable unit is a truly microscopic object as small as a fragment of a molecule or a single chemical bond of a network glass. The low-energy state is identified with the ideal glass, while excitations associated with molecular motions belong to a Gaussian manifold of energies with the width σ (Fig. 2). The energetic disorder arises from the local disordering field and packing restrictions around a given excitable unit.

The real-space model of two-state excitations is next projected onto Goldstein's configuration space of a liquid at constant pressure.⁵⁸ This configuration space can be separated into basins of attraction characterized by the minimum depth ϕ . We can write the excess Gibbs energy relative to the energy of the ideal-glass state (superscript "ex") as a double sum over the basin energies and the fraction of excited units x out of N excitable units

$$e^{-g^{\text{ex}}/NT} = \sum_{\phi} e^{-\phi/NT} \sum_{0 \leq x \leq 1} e^{s(\phi, x)}, \quad (7)$$

where^{59,60}

$$e^{s(\phi, x)} = \frac{N!}{(N-xN)! (xN)!} [(Q_v^e/Q_v^g)^x P(\phi, x)]^N. \quad (8)$$

Here, $P(\phi, x)$ is the distribution of minimum energies in configuration space obtained by projecting the excitation energy $x(\varepsilon_0 + Pv_0 + \delta\varepsilon)$ on the Gaussian manifold

$$P(\phi, x) = \int \delta[\phi - x(\varepsilon_0 + Pv_0 + \delta\varepsilon)] G(\delta\varepsilon) d\delta\varepsilon, \quad (9)$$

where $G(\delta\varepsilon)$ is a Gaussian distribution

$$G(\delta\varepsilon) \propto \exp[-(\delta\varepsilon)^2/2\sigma^2]. \quad (10)$$

All energies here and below are in kelvin, entropies and heat capacities are in units of k_B .

The ratio of vibrational-rotational partition functions $Q_v^{s,e}$ in the ground (superscript g) and excited (superscript e) states can be absorbed into the excitation entropy

$$s_0 = \ln[Q_v^e/Q_v^g] = s_0^v + s_0^c, \quad (11)$$

which is composed of the harmonic vibrational contribution, s_0^v , and a configurational contribution, s_0^c . The vibrational excitation entropy is related to the excess density of states of low-frequency vibrational modes near and below the boson peak⁶¹

$$s_0^v = \sum_{\omega} (g_{\omega}^e - g_{\omega}^g) \ln[\omega]. \quad (12)$$

In Eq. (12), the sum runs over the vibrational frequencies ω (eigenvalues of the Hessian matrix) with the densities of vibrational states in the ground and excited states $g_{\omega}^{s,e}$.

The thermodynamic limit $N \rightarrow \infty$ transforms the entropy $s(\phi, x)$ in Eq. (7) into a sum of the ideal mixing entropy, $s_0(x)$, and a Gaussian term⁵⁷

$$s(\phi, x) = s_0(x) - \frac{[\phi - x(\varepsilon_0 + Pv_0)]^2}{2x^2\sigma^2}, \quad (13)$$

where

$$s_0(x) = xs_0 - x \ln(x) - (1-x) \ln(1-x). \quad (14)$$

The sum over x in Eq. (7) is determined by its largest summand at $x=x(\phi)$. One then arrives at the landscape thermodynamics in which the thermodynamic observables are determined by the excess free-energy function depending on ϕ (we omit the dependence on P for brevity)

$$g^{\text{ex}}(\phi) = \phi + e_{\text{anh}}^{\text{ex}}(\phi) - Ts^{\text{ex}}(\phi), \quad (15)$$

$$s^{\text{ex}}(\phi) = s[\phi, x(\phi)],$$

where $e_{\text{anh}}^{\text{ex}}(\phi)$ is the energy related to the anharmonicity effects not included in the harmonic approximation (entropy from anharmonicity is small as indicated by computer simulations³⁰). The excess free energy $g^{\text{ex}}(\phi)$ is composed of the configurational and vibrational parts

$$g^{\text{ex}}(\phi) = g_c(\phi) + g_v(\phi), \quad (16)$$

where

$$g_v(\phi) = e_{\text{anh}}^{\text{ex}}(\phi) - x(\phi)s_0^vT. \quad (17)$$

One can alternatively consider the sum over ϕ in Eq. (7) that maximizes at the average basin energy $\langle\phi(x)\rangle$. The (partial) Gibbs energy can be considered as a function of the population

$$g^{\text{ex}}(x) = \langle\phi(x)\rangle + e_{\text{anh}}^{\text{ex}}[\langle\phi(x)\rangle] - Ts[\langle\phi(x)\rangle, x]. \quad (18)$$

The minimum of $g^{\text{ex}}(x)$ gives the thermodynamic Gibbs energy g^{ex} in Eq. (7). The formulation in terms of $g^{\text{ex}}(x)$ is thermodynamically equivalent to the landscape thermodynamics in terms of $g^{\text{ex}}(\phi)$ since the thermodynamic Gibbs energy g^{ex} is achieved at the largest summand in both x and ϕ in the double sum in Eq. (7). We will, however, obtain both $g^{\text{ex}}(\phi)$ and $g^{\text{ex}}(x)$ in order to gain better insight into the physics of the model.

The excitation energy ε_0 can, to the first approximation, be considered as independent of temperature. The situation is quite different with the Gaussian width σ^2 [Eq. (10)]. The energy of the localized excited state is randomized by interactions with the thermal motions of the liquid which are not quenched and therefore affected by temperature. The fluctuation-dissipation theorem then requires that $\sigma^2 = 2\lambda T$ scales linearly with temperature,^{62,63} as does the mean-square displacement of a classical harmonic oscillator, $\langle x^2 \rangle \propto T$. Here, λ is the trapping energy or the energy of stabilization of an excitation by the disorder of the medium in which it exists.^{50,64} Once this real space Gaussian width is substituted into Eqs. (8) and (10), it results in an approximately linear temperature scaling of $\langle(\delta\phi)^2\rangle$ [which is more complex because of a generally nonparabolic form of $g^{\text{ex}}(\phi)$ and temperature dependence of the population x].⁵⁷

The notion of the linear ($\propto T$) temperature dependence of $\langle(\delta\phi)^2\rangle$ (which we will verify later) is one of the central components of the present model.⁵⁷ The energy landscape of the system, i.e., energy as a function of $3N$ coordinates of the molecules making up the liquid, is determined by intermolecular interactions and is expected to be weakly temperature dependent at constant volume of the liquid. However, when the manifold of all possible states in $3N$ space is projected onto one single coordinate of the basin energy ϕ , the distribution of ϕ , given in terms of the (partial) free energy $g^{\text{ex}}(\phi)$, gains temperature dependence. Not only the first moment of this distribution, the average basin energy, is temperature dependent, as indeed described by random-energy models,⁶⁵ but essentially all higher moments are temperature dependent as well. The random-energy model, originally developed for spin glasses,⁶⁶ assumes that the width of the Gaussian distribution of random spin configurations is independent of temperature. This assumption is well justified for systems with quenched disorder, but probably not as well for liquids in a metastable (slow nucleation) equilibrium. Likewise the original Stillinger–Weber formulation⁶⁷ assumed that temperature affects only the average energy $\langle\phi\rangle$ in the form of “descending into the landscape” but not any higher moments of the distribution. The simulation evidence on this matter is insufficient and somewhat controversial. While some simulations of small ensembles of binary Lennard-Jones^{7,8,68,69} (LJ) and dipolar⁷⁰ fluids give clear indication of an approximately linear dependence of $\langle(\delta\phi)^2\rangle$ on

T , simulations of larger LJ ensembles give virtually constant width.⁴² This distinction is not accidental. The width of the distribution of inherent structures scales as $1/\sqrt{N}$ and needs to be measured on small ensembles.

The ideal-glass state should in principle involve randomness (simulations for network liquids show a finite configurational entropy at the cutoff energy⁷¹) and the previous version of the model⁵⁷ (2G model) assumed Gaussian distributions for both the ideal glass energies and the excited configurations with the widths $\sigma_i^2 = 2k_B T \lambda_i$ ($i=1, 2$). However, as we noted in Ref. 57, the fit of the 2G model to experimental heat capacities and configurational entropies resulted in a small and almost constant $\lambda_1 \approx 15-40$ K for the ideal-glass state. The application of the model to a more extensive list of glass-forming liquids performed in this paper has shown that λ_1 can be set equal to zero without sacrificing the quality of the fit. This will be the model adopted here. This version of the model, with only one Gaussian manifold for the configurationally excited states, will be referred to as the 1G model. The random energy statistics we consider here have much in common with the model of protein folding proposed by Bryngelson and Wolynes^{59,72} and the equations we derive share features with the earlier cooperative two-state model of Strässler and Kittel⁷³ (which is a forerunner of the two species nonideal liquid model of Rapoport,⁷⁴ the “two liquids” model of Aptekar⁷⁵ and Ponyatovsky and co-workers,⁷⁶ and the cooperative defects models of Granato⁷⁷ and of Angell–Moynihan⁷⁸).

Now we turn to the thermodynamics of configurational excitations. The excess Gibbs energy $g^{\text{ex}}(\phi)$ minimizes at the average basin energy

$$\langle \phi \rangle = x(\varepsilon_0 + P v_0) - 2x^2 \lambda (1 + \partial e_{\text{anh}}^{\text{ex}} / \partial \phi). \quad (19)$$

In what follows we will neglect the generally unknown derivative $\partial e_{\text{anh}}^{\text{ex}} / \partial \phi$. This approximation is expected to be accurate at low temperatures close to T_g , but will fail at higher temperatures above the onset temperature at which the system starts to descent into the energy landscape. In this approximation, the excited-state population is defined by the self-consistent equation

$$x = [1 + e^{g_0(x)/T}]^{-1}, \quad (20)$$

where the free energy per excitable unit is

$$g_0(x) = \varepsilon_0(x) - T s_0. \quad (21)$$

Because of the energetic disorder of the excited states the actual excitation energy is lowered by twice the trapping energy 2λ .^{57,79} However, only configurationally excited states can “solvate” (stabilize) the excitation and the stabilization energy is proportional to the population x of the excited states. The effective excitation energy $\varepsilon_0(x)$ in Eq. (21) and Fig. 2 then becomes

$$\varepsilon_0(x) = \varepsilon_0 + P v_0 - 2x\lambda, \quad (22)$$

where the factor of 2 comes from counting all interactions of a given unit with the rest of the ensemble of configurational excitations.

By relating x to the spin variable $\sigma = 2x - 1$, Eq. (20) can be brought to the form usually considered by models of ferromagnetism⁸⁰

$$\sigma = \tanh \left[\frac{\lambda \sigma}{2T} - \frac{g_0 - \lambda}{2T} \right], \quad (23)$$

where the excess Gibbs energy of configurational excitations is

$$g_0 = \varepsilon_0 + P v_0 - T s_0. \quad (24)$$

At $s_0 = 0$ and $\lambda = \varepsilon_0 + P v_0$ Eq. (23) transforms into the Weiss formula for spontaneous magnetization⁸⁰ with $\lambda \sigma / 2$ playing the role of the effective field of the magnetic moments.

The self-consistent equation for the population of configurational excitations [Eq. (20)] bears some similarity with the results of previous studies minimizing the mean-field free-energy functionals of liquid-state theories. The density of the liquid $\rho(\mathbf{r})$ can then be found from the self-consistent equation^{81,82}

$$\rho(\mathbf{r}) = q \exp \left[\int c(\mathbf{r} - \mathbf{r}') \rho(\mathbf{r}') d\mathbf{r}' \right], \quad (25)$$

where q is the activity and $c(\mathbf{r})$ is the direct correlation function. Solution of this equation predicts a first-order transition to aperiodic crystal.⁸¹ Molecular dynamics simulations, however, indicate⁸³ that a kinetic transition happens before the thermodynamic transition is reached, in qualitative agreement with our analysis of experimental data (see later).

The combination of the average energy [Eq. (19)] and excess entropy [Eqs. (13) and (15)] as functions of population yields $g^{\text{ex}}(x)$ in Eq. (18)

$$g^{\text{ex}}(x) = x g_0 - x^2 \lambda + e_{\text{anh}}^{\text{ex}}[\langle \phi(x) \rangle] + T [x \ln x + (1-x) \ln(1-x)]. \quad (26)$$

Except for the anharmonic correction, this equation has been derived in many previous publications.^{73-76,84} Minimization of $g^{\text{ex}}(x)$ with respect to x (neglecting the derivative $\partial e_{\text{anh}}^{\text{ex}} / \partial x$) leads to Eq. (20). The parameter λ then plays the role of the average energy of interaction between the configurational excitations. Consequently, the quadratic in x term in Eqs. (19) and (26), originating from the energy randomness in our model, is equivalent to direct mean-field (Bragg–Williams⁸⁰) interaction between the excited units. In other words, randomness is effectively equivalent to attraction when separate units independently seek the same satisfactory configuration.⁷⁹ Notice that derivation of Eq. (26) requires the explicit account of the linear temperature scaling of the real-space Gaussian width σ^2 in Eq. (10). The assumption of a temperature-independent width would result in a $1/T$ scaling of the energy term in $g^{\text{ex}}(x)$ quadratic in x .

Since the full calculation of the excess thermodynamics of the supercooled liquid over its crystal is too a complex task even for phenomenological models we next assume that the configurational entropy of two-state excitations, $s^{\text{ex}}(T)$, gives the excess entropy of the liquid over its crystal. We will use this excess entropy for the rest of our thermodynamic analysis warning at this point that this entropy, not being the thermodynamic entropy, is not thermodynamically

consistent with the excess Gibbs energies in Eqs. (15) and (26), i.e., $s^{\text{ex}}(T) \neq -[\partial g^{\text{ex}}(T)/\partial T]_p$. A thermodynamically consistent $g^{\text{ex}}(T)$ can of course be obtained by temperature integration of $s^{\text{ex}}(T)$.

According to our derivation above, $s^{\text{ex}}(T)$ is the sum of the configurational entropy $s_c(T)$ and the vibrational entropy $x(T)s_0^v$,

$$s^{\text{ex}}(T) = s\{\langle\phi[x(T)]\rangle, x(T)\} = s_c[x(T), T] + x(T)s_0^v, \quad (27)$$

where $\langle\phi[x(T)]\rangle$ and $x(T)$ are given by Eqs. (19) and (20), respectively. The configurational entropy thus accommodates only that part of s_0 which is not related to the change in the vibrational density of states. It is given as a sum of the ideal mixture entropy $s_0^c(x)$ and the fluctuation entropy $-x^2\lambda/T$ consequent on the shrinking of the Gaussian width with decreasing temperature⁵⁷

$$s_c(x, T) = s_0^c(x) - x^2\lambda/T, \quad (28)$$

where

$$s_0^c(x) = xs_0^c - x \ln x - (1-x)\ln(1-x). \quad (29)$$

B. Application to experimental data

We now proceed to applying the model to laboratory and simulation data for supercooled molecular liquids. In the former case, excess entropy Δs of the liquid over the crystal is identified with the excess entropy over the ideal-glass state $s^{\text{ex}}(T)$ [Eq. (27)]. In the case of simulations, conjugate gradient minimization of simulated trajectories allows sampling of inherent structures and equations for the configurational component of the excess entropy will be used [Eqs. (28) and (29)]. The two sets of equations are formally equivalent when the overall excitation entropy s_0 is used for the excess data and only its configurational component s_0^c is used for the statistics of inherent structures.

No progress can be made without recognizing that the molar quantity, heat capacity, determined in a laboratory measurement contains contributions from z “rearrangeable subunits” of the molecule which are the microscopic dynamic elements of the system. This is most obvious in the case of chain molecule systems like selenium or like 4-methyl nonane⁴⁰ where each methyl group constitutes one “bead” according to Wunderlich’s original description.⁸⁵ The number of subunits or beads per molecule is not always evident. In selenium the atom is clearly the bead but in the glass-former 9-bromo phenanthrene,⁸⁶ the whole C_{20} “raft” is rigid and can only rearrange as a single unit.

Stevenson and Wolynes have suggested an operational approach to determining z , based on the entropy of fusion relative to that of the simple LJ system.⁸⁷ While this method does not take account of the fact that the LJ fusion entropy is determined at a temperature where the liquid is enormously more fluid than the glass formers at their melting points (entropy per bead $1.68k_B$ compared to Wunderlich’s $1.36k_B$, which leads to gross overestimates in the case of low fusion entropy network liquids, e.g., $ZnCl_2$), it does give a measure that is roughly consistent with others. These range from the original Wunderlich⁸⁵ and Privalko⁴⁰ estimates, through

TABLE I. Number of excitable units (beads) per mole of a glass former. The last column represents the effective number of classical oscillators in a molecule (mole) of a substance at T_g .

Substance	Privalko ^a	Takeda ^b	Moynihan ^c	Stevenson ^d	$C_p^{\text{ex}}(T_g)/3$
Inorganics					
Se	1	1	1	0.9	1
$ZnCl_2$	1			1.2	3
Aromatics					
Toluene	4		1	2.7	3.2
<i>o</i> -terphenyl (OTP)	9		2	3.7	
Paraffinics					
2-methylpentane	6		3	3.8	3.2
Alcohols					
Methanol	2	2		1.3	1.76
Glycerol	6	6	7	4.5	3.5
Hydrates					
$Ca(NO_3)_2 \cdot 4H_2O$	13			7.0	11.7

^aSee Ref. 40.

^bSee Ref. 88.

^cSee Ref. 54.

^dSee Ref. 87.

Takeda *et al.* based on structural arguments⁸⁸ down to Moynihan and Angell whose estimates were based on best fitting of the excess entropy to an excitations model.⁵⁴ Some comparisons are provided in Table I.

The separation of a molecule into z statistically independent subunits neglects the finite correlation length of the disordering field. Indeed, if two units are within the field’s correlation length, they contribute to the statistics of basins as a single unit. The number of units z is thus an effective parameter necessarily smaller or equal to the number of conformationally distinct units (cf. the difference between Privalko’s conformational and Stevenson’s effective numbers in Table I). Because of its effective nature, z can be represented by fractional numbers as was done by Stevenson and Wolynes (Table I). Although this approach provides more flexibility in fitting the experiment, we will follow here Takeda *et al.*⁸⁸ and Moynihan and Angell⁵⁴ and use integral numbers for z . In order to distinguish between thermodynamic properties referring to excitable units and molecules (or generally moles), we will use lower-case letters for the former and upper-case letters for the latter. Lower-case and upper-case extensive variables are connected through z , e.g., for the constant-pressure heat capacity, $C_p = zc_p$.

We will apply the model to constant-pressure data and consider the excitation energy ε_0 as an adjustable parameter. Therefore, for the rest of our analysis, the term Pv_0 in the excess Gibbs energy [Eq. (24)] is fused into ε_0 . Therefore, given the number of excitable units per molecule z has been specified, the 1G model contains three model parameters, ε_0 , λ , and s_0 . We have tested the model for a set of glass formers identified as fragile (strong super-Arrhenius kinetics, from toluene to salol) and intermediate (weak super-Arrhenius kinetics, from 3-bromopentane to *n*-propanol) liquids. Results shown in Fig. 3 and listed in Table II were obtained from a simultaneous fit of the model to excess heat capacities and

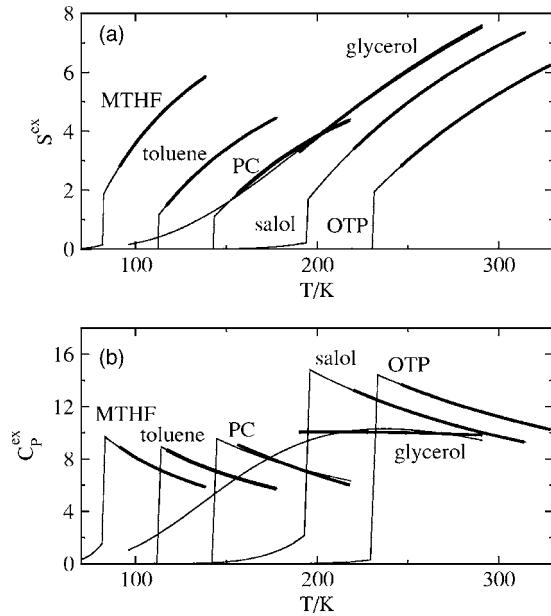


FIG. 3. Excess entropy (a) and excess heat capacity (b) for some of the supercooled liquids listed in Table II (per molecule, in units of k_B). The thin lines refer to fits to the 1G model, the thick lines refer to the experimental data (see Ref. 54).

entropies from Ref. 54, bound by the constraint $\varepsilon_0(x) \geq 0$ [Eq. (22)] required for the mechanical stability of the ideal-glass state.

The experimental excess entropies are calculated from the constant-pressure heat capacity $C_P^{\text{ex}}(T)$ and the fusion entropy ΔS_{fus} according to the relation

$$S^{\text{ex}}(T) = \Delta S_{\text{fus}} + \int_{T_{\text{fus}}}^T C_P^{\text{ex}}(T') (dT'/T'), \quad (30)$$

where T_{fus} is the fusion temperature and $S^{\text{ex}}(T) = z s^{\text{ex}}(T)$. The number of excitable units per molecule (mole) z was taken from Moynihan and Angell⁵⁴ and varied additionally to find the best-fit integral numbers. Equal quality fits can be ob-

tained in some cases with different numbers z , e.g., for toluene $z=1$ and $z=2$ can be adopted. In that latter case, $z=1$ was taken to maintain the consistency of parameter values with other fragile liquids (Table II). The choice of z here does not affect our qualitative conclusions discussed later.

The constant-pressure heat capacity, used to fit the experimental data, was obtained by the direct differentiation of the excess entropy constrained by the assumption that the trapping energy λ is independent of temperature. This assumption is supported by spectroscopic studies showing weak dependence of the Stokes shift (which is an analog of the trapping energy for electronic transitions) on temperature.⁹¹ With this assumption one gets

$$c_P^{\text{ex}} = \frac{x^2 \lambda}{T} + x(1-x) \frac{\varepsilon_0(x) [\varepsilon_0(x) - 2x\lambda]}{T^2 [1 - x(1-x)(2\lambda/T)]}. \quad (31)$$

At $\lambda=0$ this equation reduces to Schottky's heat capacity $c_P^{\text{ex}} = x(1-x)(\varepsilon_0/T)^2$, which is further reduced to the Hirai-Eyring equation,⁹² proposed on the basis of transition-state ideas, in the limit $x \ll 1$. For fragile liquids, $x \approx 1$, as we show later, and the heat capacity becomes

$$c_P^{\text{ex}} = \lambda/T. \quad (32)$$

Notice that Eq. (31) anticipates a Curie type, $(T-T_c)^{-1}$, divergence of the heat capacity at the critical temperature defined by the equation $T_c = 2\lambda x(T_c) [1 - x(T_c)]$.

The fragility of a glass former is often characterized by the steepness index^{1,2}

$$m = d \log \pi/d(T_g/T)|_{T=T_g} \quad (33)$$

(listed in Table II) or by its thermodynamic equivalent.^{93,94} What appears to be a smooth transition from fragile salol to intermediate 3-brombenzene according to the steepness index in fact corresponds to a drastic decrease in the trapping energy by a factor of about 50. Low values of λ turn out to be characteristic of all intermediate liquids in Table II. The result is a profound change in the relative importance of the

TABLE II. Best-fit parameters of the 1G model to experimental excess entropies and heat capacities. Also shown are the experimental Kauzmann temperature T_K^{exp} obtained by extrapolating experimental entropies to zero (Ref. 54) and by using Eq. (38), experimental VFT temperature T_0 , and the thermodynamic Kauzmann temperature T_K calculated from Eq. (4) using the 1G excess entropy from Eqs. (27) and (29). The temperature of liquid-liquid transition T_{LL} is calculated from Eq. (34), T_g is the experimental glass transition temperature. All energies and temperatures are in kelvin, the entropy s_0 is in k_B units.

Substance	$m^{a,b}$	z^c	ε_0	λ	s_0	T_K^{exp}	T_0^b	$T_K^{\text{exp},d}$	T_{LL}	T_K^e	T_g
Fragile liquids											
Toluene	105 ^f	1	2171	1020	10.2	100	96.5 ^e	100	113	108	117
<i>D, L</i> -propene carbonate	104	1	2921	1383	10.7	129		129	144	123	156
OTP	81	2	3576	1686	8.3	204	202.4	206	228	170	246
2-methyltetrahydrofuran (MTHF)	65	2	899	414	5.9	69	70	70	82	50	91
Salol	63	3	2070	988	5.6	175	175	176	193	115	220
Intermediate liquids											
3-bromopentane (3BP)	53	4	348	20	2.0	84	83			75	108
Glycerol	53	7	738	5.0	1.6	137	130 ^e			59	190
<i>n</i> -propanol (nPOH)	35	2	406	22	2.8	72	70			30	96

^aSteepness fragility index, Eq. (33).

^bTaken from Ref. 27 unless indicated otherwise.

^cFrom Ref. 88.

^dCalculated from Eq. (38).

^eObtained as the temperature of crossing zero for the excess entropy calculated in the 1G model.

^fReference 89.

^gReference 90.

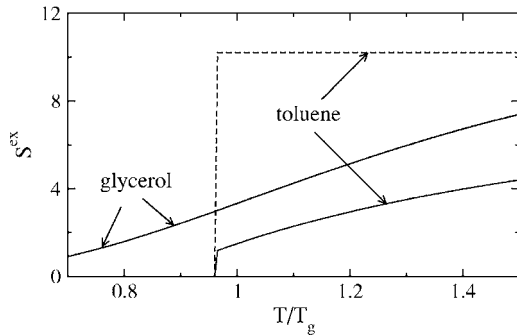


FIG. 4. Excess entropy (solid lines) and its ideal-mixture component $z s_0(x)$ (dashed lines) [Eq. (14)] vs temperature. The dashed and solid lines coincide on the scale of the plot for glycerol.

ideal mixing and Gaussian terms in the excess entropy.

For fragile liquids, the ideal mixing entropy [Eq. (14) or Eqs. (27) and (29)] is large and is almost constant in the whole temperature range of a supercooled liquid $T_g \leq T \leq T_m$ (toluene in Fig. 4). This is a reflection of the fact that the population of the high-energy state, driven by the excitation entropy s_0 , is close to unity⁹⁵ and almost independent of temperature. The excess ideal mixing entropy is finally lost in a first-order transition to a low-entropy liquid state at a temperature T_{LL} which, according to fits to experimental data, lies between the Kauzmann temperature T_K and T_g (see Table II). The temperature of the equilibrium phase transition is defined in terms of the model parameters as

$$T_{LL} = \frac{\varepsilon_0 - \lambda}{s_0}. \quad (34)$$

This first-order transition [Fig. 5(a)] gives rise to a pretransitional rise of the heat capacity which is cut off by the kinetic glass transition at T_g . The observed drop of the heat capacity is related to the loss of ergodicity which we do not consider here. The entropy does not drop to zero at T_{LL} but in all cases becomes small, crossing zero at the Kauzmann temperature T_K much below the experimental temperature T_K^{exp} (Table II). A second order phase transition can be realized at the critical point when the excitation energy gap is related to the trapping energy by the following equation:⁷³

$$\varepsilon_0 = \lambda + \lambda s_0/2. \quad (35)$$

However, when this restriction is imposed on the parameters, the model fails to fit the experimental data.

The physics is quite different for intermediate liquids for which the ideal mixture term provides the main part of $s^{ex}(T)$. The excess entropy then decreases with temperature due to decreasing population of the excited state, which cannot stay at a high value because of a smaller entropy gain s_0 compared to fragile liquids (glycerol in Fig. 4). The entropy smoothly decreases without a discontinuity related to thermodynamic phase transition [see Fig. 5(b) for the illustration of various temperatures used in the present thermodynamic analysis].

The disappearance of the first-order transition for nonfragile (strong and intermediate) liquids is related to two critical parameters, critical temperature T_c and critical exci-

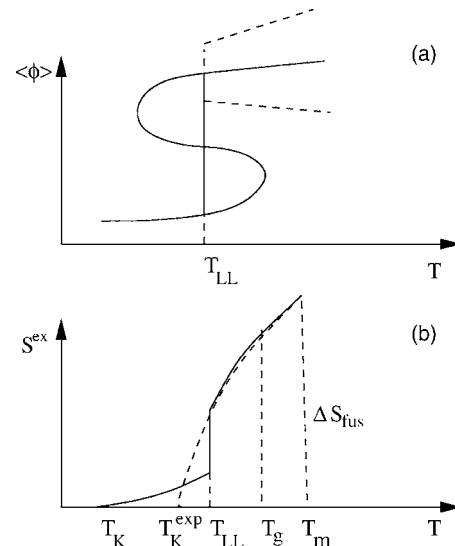


FIG. 5. Temperature dependence of the average basin energy (a) and excess entropy (b) of fragile glass-formers. The almost flat dependence of the average energy on temperature is terminated by discontinuous first-order phase transition at temperature T_{LL} . At this temperature the excess entropy, as predicted by the 1G model [solid line in (b)], also shows a discontinuous drop to a nonzero value which decays to zero at the thermodynamic Kauzmann temperature T_K . The broken line in (b) illustrates the experimental interpolation of the high-temperature $1/T$ law ending up at the experimental Kauzmann temperature T_K^{exp} . The dashed lines in (a) indicate the narrowing of the Gaussian distribution of excitation energies with decreasing temperature.

tation entropy s_{0c} . A first-order phase transition is possible for temperatures below T_c and entropies higher than s_{0c} (see Ref. 57),

$$T < T_c, \quad s_0 > s_{0c}, \quad (36)$$

where

$$T_c = \lambda/2, \quad s_{0c} = 2\varepsilon_0/\lambda - 2. \quad (37)$$

At least one of two inequalities in Eq. (36) is violated for nonfragile liquids as a result of low excitation entropies s_0 and trapping energies λ .

In parallel to the excess entropy, the average basin energy $\langle \phi \rangle$ shows qualitatively different temperature behavior for fragile and intermediate liquids. With temperature decreasing, $\langle \phi \rangle$ from Eq. (19) starts to dip as $1/T$ from a high-temperature plateau (like binary LJ fluid) and then inflects into an exponential temperature dependence $\propto \exp(-\varepsilon_0/T)$ for $\varepsilon(x)/T \gg s_0$. Both the $1/T$ decay at relatively high temperatures^{30,33,68,96} and exponential decay at low temperatures (for a model network fluid⁹⁷) have been observed in simulations. In our model, this pattern describes nonfragile liquids. For fragile liquids, the excited state population is almost constant, $x \approx 1$, in the entire range of experimentally accessible temperatures down to the glass transition. The average basin energy is constant as well, $\langle \phi \rangle = \varepsilon_0 - 2\lambda$. For infinitely slow cooling [and rare cases like triphenyl phosphite (TPP)], the population sharply changes at the liquid-liquid transition resulting in a discontinuous dip of the average energy $\langle \phi \rangle$ from its plateau value.

The temperature dependence of the excess entropy of fragile liquids above T_g is mostly determined by the $1/T$

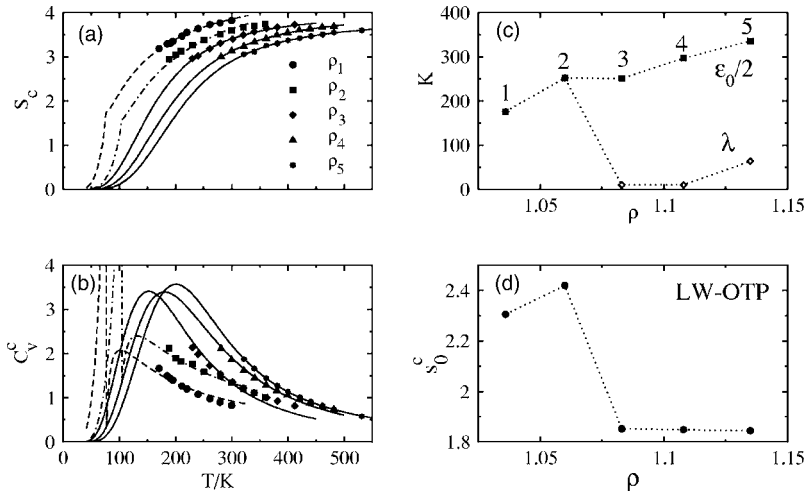


FIG. 6. Configurational entropy (a), configurational constant-volume heat capacity (b), and the fitted excitation parameters (c) and (d) for LW *o*-terphenyl ($z=2$ is used as in the case of laboratory *o*-terphenyl, Table II). The points in (a) and (b) are the simulation data from Ref. 30 at the densities indicated in (c). The dotted lines in (c) and (d) connect the points. In (c), λ is indistinguishable from $\varepsilon_0/2$ on the scale of the plot for two lowest densities. The lines in (a) and (b) are simultaneous fits of the simulated configurational entropy and heat capacity to the 1G model; the dashed and dash-dotted lines are used for two lowest densities with high fragility to distinguish them from higher densities with intermediate fragility.

decay of the second fluctuation term in Eq. (28). The result is the overall temperature dependence in the form of Eq. (6) with $S_0 = z s_0$. The experimental Kauzmann temperature is then obtained by extrapolating Eq. (6) to zero entropy, which leads, in terms of the model parameters, to the following relation:

$$T_K^{\text{exp}} = \frac{\lambda}{s_0}. \quad (38)$$

Equation (38) holds quite well for the fit parameters in Table II. In addition, the constant-pressure heat capacity scales as $1/T$ [Eq. (32)]. Therefore, parameter λ can be set by the heat capacity at the glass transition

$$\lambda = T_g c_P^{\text{ex}}(T_g). \quad (39)$$

The fit of experimental data for fragile liquids shows that ε_0 is close to 2λ and in fact can be put equal to 2λ without sacrificing the accuracy of the fit. As a result, the thermodynamics of fragile liquids is defined by the following relations often used empirically:^{21,27,87,88,98}

$$\begin{aligned} s^{\text{ex}}(T) &= c_P^{\text{ex}}(T_g) (T_g/T_K^{\text{exp}} - T_g/T), \\ c_P^{\text{ex}}(T) &= c_P^{\text{ex}}(T_g) (T_g/T). \end{aligned} \quad (40)$$

We note that random energy models, which do not anticipate temperature variation of the width of basin energy distribution,⁶⁵ result in T^{-2} scaling of the heat capacity inconsistent with Eq. (40).

It is obviously significant for our discussion to compare the results of fitting the model to laboratory excess entropies with analogous fits to configurational entropies from simulations. The Lewis and Wahnström (LW) model of *o*-terphenyl studied in Refs. 30 and 41 provides us with such an opportunity. Figure 6 shows the fit of the 1G model to the configurational entropies and heat capacities of LW *o*-terphenyl at five different densities.³⁰ The number $z=2$ is maintained equal to the analysis of experimental data to access the fraction of configurational excitation entropy in s_0 . Two main results follow from the fit: (i) the 1G model predicts the existence of a critical λ singularity below T_g for two lowest densities and its disappearance at higher densities and (ii) the configurational component of the excitation entropy follow-

ing from the fit, $s_0^c \approx 2$, is significantly lower than $s_0 \approx 8$ obtained for laboratory *o*-terphenyl (Table II). The appearance of the divergence at lower densities is the result of very close fulfillment of Eq. (35) for the fitting parameters, which is remarkable, given that the excitation parameters are freely varied in the fit. The magnitude of the fitted excitation entropy suggests that a major portion of s_0 arises from a change of the vibrational density of states,^{37,38,78} as we have also learned from comparing the laboratory and simulation data for water (see later). Our result is close to Goldstein's estimate of 28% for the fraction of configurational component in the excess entropy of *o*-terphenyl.³⁵ Goldstein's calculation was based on the comparison of excess entropies of quenched and annealed glasses at T_g , $\Delta S_{QA}(T_g)$, and at 0 K, $\Delta S_{QA}(0)$. The ratio $\Delta S_{QA}(0)/\Delta S_{QA}(T_g)$, which is equal to s_0^c/s_0 in the 1G model, gives the configurational fraction of the excess entropy.

The fit of the 1G thermodynamic model to the experimental data (Table II) shows that the thermodynamic Kauzmann temperature T_K [Eq. (4)] is significantly lower than the experimental Kauzmann temperature T_K^{exp} [Eq. (6)]. This implies that the relaxation time in the Adam-Gibbs relation does not diverge at $T_K^{\text{exp}} \approx T_0$ and the link between the thermodynamics and dynamics might be more complex. The dynamic extension of the 1G model presented next places the emphasis on the configurational heat capacity, instead of the configurational entropy, as the main reason for super-Arrhenius dynamics in fragile liquids.

III. DYNAMICS OF CONFIGURATIONAL EXCITATIONS: ENTHALPIC DRIVING FORCE

A. Formulation of the model

Here we describe a dynamic model extending the thermodynamic analysis of Sec. II. Our development starts with the assumption common to all energy-trap^{9,49} and energy-diffusion⁵⁰⁻⁵² models that nonreversible events of viscous flow and diffusion⁶ occur by exciting some states within the liquid to a common energy level E_0 , which is higher than the top of the energy landscape^{61,99} (Fig. 2). These excitations occur by absorbing kinetic energy by an excitable unit (bead) from the surrounding liquid.

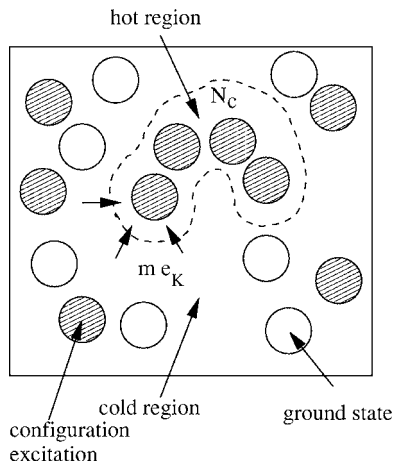


FIG. 7. Hot region of N_c configurationally excited units (hatched circles) with kinetic energy accumulated by transfer of m quanta of the kinetic energy e_K from the surrounding liquid.

We will next assume that only unjammed configurationally excited units will participate in activated events. Even when a sufficient amount of energy has been accumulated at a given unit, relaxation event may require facilitation from other units. This is particularly clear in a case of a molecule composed of z units (beads). One could imagine that, e.g., translational relaxation of such molecule would require excitation of all z units, although relaxation of conformationally flexible molecules can also proceed in a diffusive way, as a sequence of low-amplitude motions of consecutive units. Because of the assumed low amplitude of the motions involved, we will not distinguish between pairs of units within the molecule and pairs of units belonging to different molecules.

Each low-amplitude step is terminated by a transformation of the accumulated kinetic energy into a small structural change with a higher potential energy and thus higher fictive temperature. A single relaxation event requires a sequence of such locking steps by the end of which there appears a “hot” (in fictive temperature) region within the liquid which can then subsequently relax to a new configuration (Fig. 7). In this scheme the overall dynamics become hierarchical in character, the initial step being the most probable and, hence, the shortest in time. This picture is an integration of energy spikes seen in simulations of Heuer and co-workers^{96,99} with dynamical hierarchy of Palmer *et al.*¹⁰⁰ (see later).

The kinetic energy becomes increasingly scarce at low temperatures. The creation of a hot region will occur by pulling the kinetic energy from a growing number of neighboring molecules, leading to the creation of a hot island in a sea of kinetically frozen molecules (on the time scale of heat transport). This picture bears some similarity to the entropy-rich droplet enveloped by the entropy-frozen environment described by Lubchenko and Wolynes²³ and by Bouchaud and Biroli.²⁴ However, the notion of relaxation proceeding by occurrence of hot regions does not anticipate static, thermodynamically stable structures of the mosaic picture.¹⁰¹ In other words, hot regions are very improbable and contribute little to the thermodynamics of the supercooled liquid,¹⁰² which, in our picture, is dominated by single configurational excitations. The importance of hot regions is, however, am-

plified by relaxation which is critically dependent on their existence. Therefore, in contrast to the mosaic picture,^{20,22} the creation of a hot region is not identified with a minimum of the free-energy surface as a function of some “order parameter.”

Hot regions can be identified with dynamic heterogeneity, i.e., the existence of regions of markedly different mobility.^{103,104} Computer simulations generally support this view.^{31,105,106} Within this general umbrella, dynamic heterogeneity can be treated in two distinct ways: as a static distribution of relaxation times in regions of varying mobility^{21,104,107} or in a dynamic fashion as facilitated kinetics of transfer of excitations from mobile particles to their neighbors.⁵⁵ Our formulation will follow this latter pathway using the kinetic scheme of hierarchical relaxation events advanced by Palmer *et al.*¹⁰⁰

According to the hierarchically facilitated dynamics, step $n+1$ happens only when a configuration at step n is reached to facilitate the next move.¹⁰⁰ This idea has been instrumental in establishing the conceptual basis for kinetically constrained models¹⁰⁸ and, physically, leads to dynamical heterogeneity when dynamically cooperative regions in the glass are created by a sequence of constrained motions of fastest molecules in the ensemble.⁵⁵ In our model, step n is reached when n excitable units within a hot island have “blinked” into the excited state with the probability

$$P_n = (\tau_0/\tau_1)^n = \exp[\mu n], \quad (41)$$

where τ_1 is the average waiting time for a single unit and τ_0 is the same as in Eq. (2). As a result of a sequence of correlated steps, each resulting in excitation of n units out of N_c units in the hot island, the waiting time of level n becomes¹⁰⁰

$$\tau_n = \tau_0 \exp[\mu N_n] \quad (42)$$

with $N_n = n(n-1)/2$. We can now follow Brey and Prados¹⁰⁹ to obtain the normalized relaxation function

$$\phi(t) = \zeta^{-1} [E_1(te^{-\zeta}/\tau_0) - E_1(t/\tau_0)], \quad (43)$$

where $E_1(z)$ is the exponential integral function,

$$\zeta = \mu N_{\max}, \quad (44)$$

and

$$N_{\max} = N_c(N_c - 1)/2. \quad (45)$$

For most practical purposes the relaxation function in Eq. (43) is indistinguishable (Fig. 8) from the KWW function in Eq. (1). In the intermediate range of times, $1 \ll t/\tau_0 \ll e^\zeta$, which can be very broad since $\zeta \gg 1$ for real systems, $\phi(t)$ follows the logarithmic decay, $\phi(t) \approx 1 - \ln(t/\tau_0)$, common for biopolymers.¹¹⁰ The average relaxation time $\tau = \int_0^\infty t \phi(t) dt$ from Eq. (43) is

$$\tau = (\tau_0/\zeta)(e^\zeta - 1) \approx \tau_0 e^\zeta. \quad (46)$$

Notice that the KWW function is more flexible than Eq. (43) because it involves two free parameters, τ/τ_0 and β , in contrast to the single parameter ζ in Eq. (43). More complex facilitation rules than the ones used here will provide additional parameters and a possibility of realizing the KWW relaxation function¹⁰⁰ which has the advantage of allowing

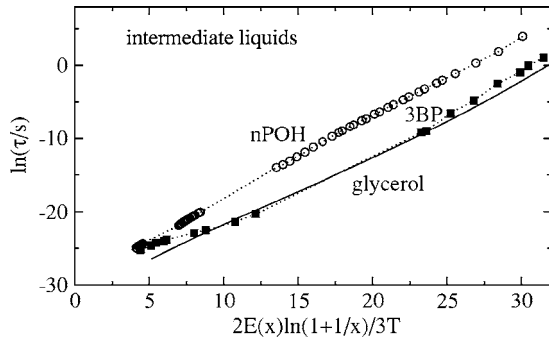


FIG. 10. Test of Eq. (54) using dielectric relaxation data for intermediate liquids listed in Table II. The high-temperature activation energy E_D in Eq. (54) is equal to $18.4T_g$ (glycerol), $22.6T_g$ (nPOH), and $16.0T_g$ (3BP) (Ref. 118). E_D for 3BP was obtained from its empirical connection to the steepness index m given in Ref. 118. The excited-state population $x(T)$ and $\Delta\phi(T)$ in Eq. (54) are calculated from the 1G model with the liquid parameters listed in Table II. The slopes of the linear regressions are 1.0 (glycerol), 1.1 (nPOH), and 1.0 (3BP). In case of glycerol, the average kinetic energy of $3T$ has been adopted.

$$\tau_1 = \tau_0 e^{\mu} = \tau_0 \int \exp[E(x)/(ze_K)] P(e_K) de_K, \quad (53)$$

where $P(e_K)$ is the distribution of the kinetic energy.

For the energy landscape characteristic of strong and intermediate liquids the canonical narrow distribution of basin energies projects itself, in the microcanonical ensemble, into a narrow distribution of kinetic energy e_K . The distribution function $P(e_K)$ in Eq. (53) can be replaced by a delta function. Assuming that the average kinetic energy is equal to $E_K = (3/2)T$ (translations for diffusion and viscous flow and rotations for dielectric relaxation), and using Eq. (51) for $E(x)$ in Eq. (53) one gets for the average relaxation time

$$\ln(\tau/\tau_0) = (2/3T)[E_D - z\Delta\phi(x)] \ln(2 + e^{-s_0 + \varepsilon_0(x)/T}). \quad (54)$$

The relaxation is Arrhenius at high temperatures [$\varepsilon_0(x)/T \ll s_0$ and $z\Delta\phi \ll E_D$]. Two things happen when the temperature is lowered. First, the energy gap between the average minimum energy $\langle\phi_m\rangle$ and the energy level e_0 starts to increase⁵² as $a+b/T$ since $\Delta\phi(x)$ scales as $1/T$ right below the onset temperature.²⁸ Second, at $\varepsilon_0(x)/T \gg s_0$ the logarithmic term in Eq. (54) generates a $1/T$ factor. Overall, the temperature law at these low temperatures becomes

$$\ln(\tau/\tau_0) = E_1/T^2 + E_2/T^3, \quad (55)$$

which is a linear combination of the Bässler⁶⁴ and Litovitz¹¹⁷ temperature laws.

This sort of non-Arrhenius kinetics is capable of describing the relaxation of intermediate liquids studied in Sec. II. Figure 10 shows experimental dielectric relaxation times²⁷ versus the right-hand side of Eq. (54) calculated from the 1G model. The parameters affecting population x are taken from our thermodynamic analysis summarized in Table II. Experimental high-temperature activation energies E_D are from Ref. 118. The analysis yields straight line with the slope 1.1 for *n*-propanol and a less clear linear trend for 3BP with the linear regression slope of 1.0. For glycerol, the slope of 1.0 is obtained by assuming the average kinetic energy equal to $3T$, which might reflect the participation of both rotational and

translational degrees of freedom in the relaxation process. We need to note that vibrational heat capacity of many glass-forming liquids does not reach the Dulong and Petit limit in its low-temperature portion. Therefore, the average kinetic energy can fall below $(3/2)T$ also becoming a nonlinear function of temperature. Accounting for this effect, which is not considered here, will make the temperature dependence in Eq. (54) even more complex.

Equation (54) is insufficient to account for super-Arrhenius behavior of fragile liquids illustrated in the upper portion of Table II and it does not help to account for the empirical connection between kinetic and thermodynamic properties of glass formers³ which the Adam–Gibbs equation (hence, also the entropic droplet model) anticipates. This is because, as we noted earlier (and has been expected on general grounds^{16,55}), the rare kinetic events in our model are essentially disconnected from the thermodynamics described here by the statistics of two-state excitations. It is important to see, then, how this correlation can arise from the present model.

It comes from the way in which the Gaussian width of the excitations distribution changes with temperature, (a key distinction between this and previous landscape models), and consequently how the system “becomes conscious” of the ruggedness of its energy landscape as temperature decreases. At high temperatures, the distribution of basin energies is wide and there is always a sufficient number of initial states contributing to the high-temperature activated relaxation with the barrier e_D in Fig. 2. As the temperature decreases, the distribution narrows and the system starts utilizing initial states lying within the rugged landscape of low-energy basins. Thus as temperature decreases, the fluctuations in the kinetic energy between the vibrational (kinetic energy) and configurational manifolds [Eq. (53)], involved in maintaining ergodicity, become increasingly important. e_K in Eq. (53) can be connected to the fluctuation of the energy of inherent structures by assuming that the average energy is $\langle E \rangle = (3/2)T + z\langle\phi\rangle$. The instantaneous kinetic energy is then

$$E_K = (3/2)T - z\delta\phi, \quad (56)$$

where $\delta\phi = \phi - \langle\phi\rangle$. The distribution of $\delta\phi$ is Gaussian

$$P(\delta\phi) = (2\pi c_p^c T^2)^{-1/2} \exp\left[-\frac{(\delta\phi)^2}{2c_p^c T^2}\right]. \quad (57)$$

This follows from the bilinear expansion of the enumeration function $s^c(\phi)$ in $\delta\phi$ and the use of two thermodynamic identities⁶²

$$\begin{aligned} [\partial s^c(\phi)/\partial\phi]_{N,P} &= T^{-1}, \\ [\partial^2 s^c(\phi)/\partial\phi^2]_{N,P} &= -(c_p^c T^2)^{-1}, \end{aligned} \quad (58)$$

where c_p^c is the configurational heat capacity of the excitable unit [in contrast to the excess heat capacity in Eq. (31)]. Notice regarding Eq. (57) that Boltzmann statistics of the basin fluctuations follow from the hyperbolic, $c_p^c \propto 1/T$ scaling of the configurational heat capacity, while $1/T^2$ scaling of the random energy models⁶⁵ leads to the temperature-independent statistics.

The average waiting time of one-unit excitation then incorporates the thermodynamic quantity, configurational heat capacity, into the kinetics through $P(\delta\phi)$ in the integral:

$$\tau_1/\tau_0 = \int_{-\infty}^{3T/2z} \exp\left[\frac{E(x)}{3T/2 - z\delta\phi}\right] P(\delta\phi) d\delta\phi. \quad (59)$$

A simple estimate of the integral in Eq. (59) can be obtained by linearly expanding the exponent in $\delta\phi$, integrating over $\delta\phi$, and reverting to the fractional form. Combining Eqs. (44), (46), and (59), the average relaxation time of the hot region is then obtained as

$$\ln(\pi/\tau_0) = \frac{2N_{\max}E(x)}{3T - [4E(x)/9]zC_p^c(T)}, \quad (60)$$

where N_{\max} is given by Eq. (45) and the molecular (molar) configurational heat capacity $C_p^c(T)$ appears in the denominator. For fragile liquids, $E(x)$ is nearly independent of temperature down to the liquid-liquid transition point [$x \approx 1$, see Fig. 5(a)] and can be considered as constant. This consideration yields the following equation for the relaxation time:

$$\ln(\pi/\tau_0) = \frac{DT'}{T - T'C_p^c(T)}, \quad (61)$$

where the constant D is

$$D = (9/4z)N_c(N_c - 1) \quad (62)$$

and the temperature T' is described further later.

The parameters D and T' in Eq. (61) can be considered as empirical fitting quantities for the sake of interpreting the experiment. According to Eq. (32), the excess and configurational heat capacities are equal to each other for fragile liquids. The $1/T$ scaling of the configurational heat capacity then results in the overall temperature dependence of the form

$$\ln(\pi/\tau_0) = \frac{DT'T}{T^2 - z\lambda T'}. \quad (63)$$

This type of the temperature law was previously obtained for hard-sphere fluids by Jagla¹¹⁹ who combined the Adam–Gibbs formalism with an empirical equation of state. Note, however, that the configurational entropy in Jagla’s model has a $1/T^2$ temperature scaling inconsistent with the empirical $1/T$ law [Eqs. (6) and (40)].

B. Application to experimental data

Equations (61) and (63) suggest some qualitative results consistent with experimental observations. First, the model establishes a direct link between fragility and configurational/excess heat capacity. The configurational heat capacity in the denominator of Eq. (61) decreases at high temperatures, e.g., above the melting temperature T_m . Therefore, the relaxation kinetics will change from super-Arrhenius at low temperatures to Arrhenius at high temperatures.¹¹² The extent of fragile behavior is controlled by λ in the denominator of Eq. (63) which, according to our thermodynamic analysis, is large for fragile liquids, resulting in curved Arrhenius plots. Note that parameter D in Eqs. (61)

TABLE III. Best-fit parameters of Eq. (61) to experimental dielectric relaxation data with τ_0 , D , and T' considered as fitting parameters. The experimental (superscript “exp”) and calculated (superscript “calc”) pressure variation of the glass transition temperature dT_g/dP is given in K/MPa, all temperatures are in kelvin.

Substance	$\log(\tau_0/s)$	D	T'	T'^a	T'^b	dT_g/dP^{exp}	dT_g/dP^{calc}
Toluene	-15.6	145	9.3	9.8	8.7		
OTP ^c	-14.0	161	13.8	12.2	13.7	0.26 ^d	0.22
MTHF	-13.5	95.6	7.9	5.9	8.9		
Salol	-14.4	204	11.9	10.5	13.3	0.20 ^e	0.26
3BP	-13.6	209	7.1		9.4		
Glycerol	-14.2	159	13.2		10.0	0.03 ^f	0.05 ^g
nPOH	-13.2	218	7.9		6.5	0.07 ^h	0.05 ⁱ

^aCalculated for fragile liquids from Eq. (65) by applying the thermodynamic fitting parameters from Table II.

^bBased on the steepness fragility index according to Eq. (66).

^cFit to Eq. (61) for OTP was obtained by restricting $\log(\tau_0)$ to be equal to -14.

^dFrom Ref. 120.

^eFrom Ref. 121. The calculated dT_g/dP refers to $P=300$ MPa instead of atmospheric pressure in case of OTP since the data in Ref. 121 apply to high pressures only.

^fFrom Ref. 122.

^gUsing high-temperature T , P -data for viscosity from Ref. 123.

^hFrom Ref. 124.

ⁱUsing the dielectric data at 0.1 and 100 MPa from Ref. 125.

and (63) is essentially constant across all liquids studied (Table III) in contrast to parameter D in the VFT equation [Eq. (2)] which correlates with fragility. Finally, Eq. (61) predicts a return to the Arrhenius behavior³ on passing below T_g because of the drop of C_p^c which defines T_g . This feature has previously been unique to the Adam–Gibbs equation and is also shared by the random first-order transition theory.²²

In addition to providing a qualitatively correct picture, Eq. (61) performs surprisingly well in fitting the dielectric relaxation times^{27,89,90} of both intermediate and fragile liquids (Fig. 11 and Table III), as well as of simulation data (see later). Fits of experimental dielectric relaxation times to Eq. (61), with τ_0 , D , and T' considered as fitting parameters, are indistinguishable from VFT fits in all cases studied (Fig. 11, upper panel). $\ln(\tau)$ plotted against $DT'/(T - T'C_p^{\text{ex}})$ also yields straight lines and physically reasonable intercepts (Fig. 11, lower panel). The quality of the linear correlations is as good as for the Adam–Gibbs plot (cf. Figs. 11 and 12) and in some cases is even better (MTHF). Even more gratifying is the invariable slope of the plots in Fig. 11 compared to a large variance of slopes of Adam–Gibbs plots in Fig. 12. In all fits, experimental $C_p^{\text{ex}}(T)$ were used instead of $C_p^c(T)$ suggested by the denominator of Eq. (61) (in the 1G model, $C_p^{\text{ex}} \approx C_p^c$ for fragile liquids).

The nominator parameter D in Eq. (61) can be related to the average number of excitations in the hot region via Eq. (62). From Table III, we obtain $N_c \approx 10$ –20. With the usual molecular diameter of $\sigma \approx 5.5$ Å, this number projects into a length scale of ≈ 1.5 nm for a spherical cluster or larger if relaxation is facilitated through chains of molecules.³³ This length is in general accord with current estimates of spatial heterogeneities in supercooled liquids,¹²⁶ although falls below the estimate $\xi/\sigma=4.5$ given by Berthier *et al.*¹²⁷ and the random first-order transition theory.¹²⁸ The activation barrier

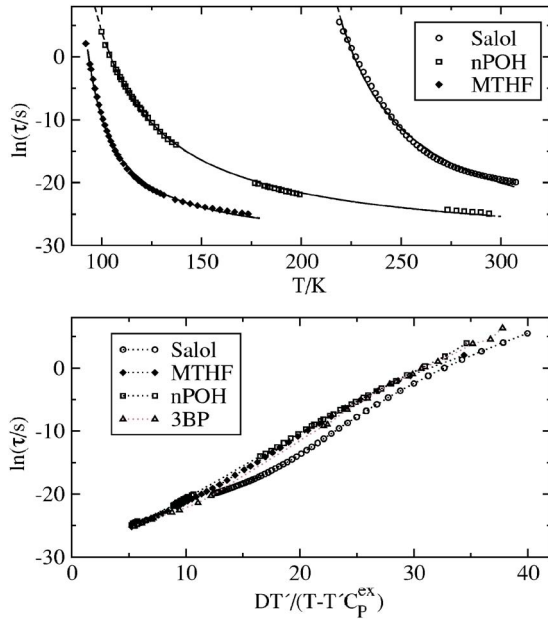


FIG. 11. Dielectric relaxation time vs T (upper panel) and vs $DT'/(T-T'C_p^ex)$ (lower panel) with D and T' listed in Table III. In the upper panel, the solid lines are fits to Eq. (61) and the dashed lines, indistinguishable from the solid lines on the scale of the plot, are the VFT fits. The intercept in the lower panel gives the physical value of 10^{-13} s.

in Eq. (61) scales quadratically with the number of units in the hot region [Eq. (62)], in contrast to the linear scaling with the number of particles in the cooperatively rearranging region of the Adam–Gibbs theory. However, there is no divergent length scale in the present formulation.

Activated dynamics considered here do not anticipate the divergence of the relaxation time at any finite tempera-

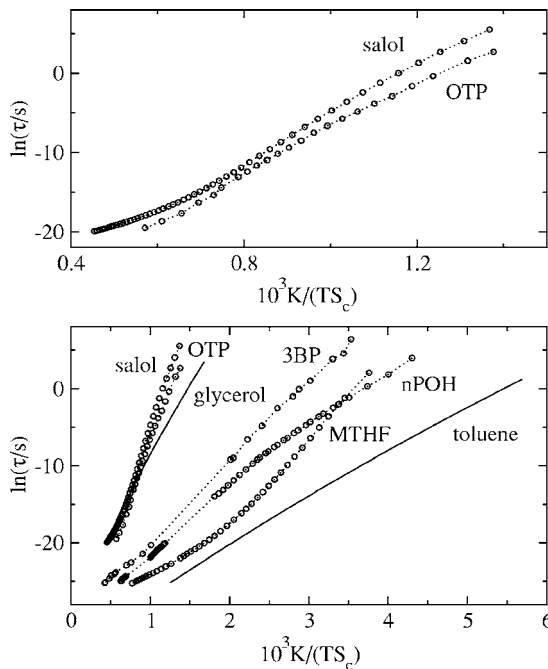


FIG. 12. Adam–Gibbs plot of dielectric relaxation time vs $[TS_c(T)]^{-1}$. The configurational entropy is calculated from the IG model with the parameters listed in Table II. The points are experimental dielectric data from Ref. 27, the solid lines are obtained by using VFT fits of the experimental data from Refs. 89 and 90.

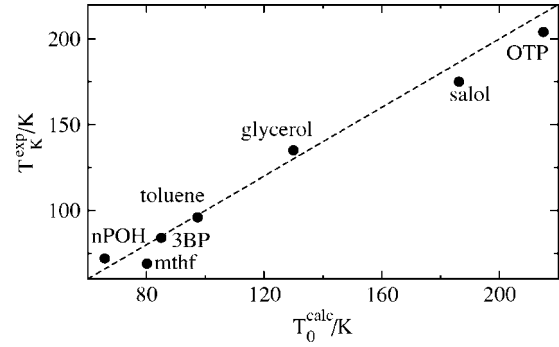


FIG. 13. Experimental Kauzmann temperature T_K^{exp} plotted against the temperature T_0^{calc} at which the relaxation time in Eq. (61) diverges. This temperature is calculated by solving Eq. (64) in which temperature T' is taken from Table III (column 4).

ture and the divergent solution given by Eqs. (61) and (63) is an artifact of the approximate integration used in Eq. (59). However, the mathematical solution of the equation

$$T_0 = T' C_p^c(T_0) \quad (64)$$

can be associated with the VFT temperature T_0 often reported experimentally. The temperature T_0 calculated from this equation (Fig. 13) is almost equal to the experimental Kauzmann temperature T_K^{exp} for all liquids listed in Table III. Equation (61) is therefore consistent with the empirically documented accord between T_0 and T_K^{exp} .⁴³

For fragile liquids, Eq. (64) simplifies to [Eq. (32), $C_p^ex \approx C_p^c$],

$$T' = \frac{T_0^2}{T_g C_p^c(T_g)} = \frac{\lambda}{z s_0^2}. \quad (65)$$

The temperature T' calculated from Eq. (65), with the thermodynamic parameters from Table II, is indeed close to the direct fit of Eq. (61) to experimental relaxation data (Table III). The parameter T' can also be related to the steepness fragility index [Eq. (33)]. Assuming T^{-1} scaling for $C_p^c(T)$ in Eq. (61), one gets

$$T' = \frac{T_g}{C_p^c(T_g)} \frac{m - m_{min}}{m + m_{min}}, \quad (66)$$

where $m_{min} = \log[\tau(T_g)/\tau_0] \approx 16$. Estimates of T' based on this equation are also listed in Table III. Since, for fragile liquids, T' is related to observable quantities through Eq. (65), one can derive the following relation for the kinetic fragility:

$$\frac{m}{m_{min}} = \frac{1 + (T_0/T_g)^2}{1 - (T_0/T_g)^2}. \quad (67)$$

This equation, which was previously derived by Ruocco *et al.*,¹²⁹ holds reasonably well for fragile liquids ($m > 53$). It makes a connection between the steepness index and the ratio T_0/T_g recommended by some authors as a measure of fragility.¹³⁰

Since the configurational heat capacity of fragile liquids is linearly related to the configurational entropy, $s_c = s_c^0 - c_p^c(T)$, Eq. (61) can be rewritten in terms of the configurational entropy

$$\ln(\pi/\tau_0) = \frac{DT'}{T + T'(S_c - z s_0^c)}. \quad (68)$$

The current formulation still provides a link between the relaxation time and configurational entropy, but the algebra is different from the Adam–Gibbs relation [Eq. (3)]. The validity of either functional dependence of the relaxation time is often tested by calculating the slope of the glass transition temperature with pressure. Equation (61) suggests that $T/T' - C_p^c(T)$ remains constant at the glass transition temperatures measured at different pressures. Following Goldstein,^{16,44} the condition $d[T/T' - C_p^c(T)] = 0$ provides the slope of the glass transition temperature with pressure, dT_g/dP . One needs to calculate the derivative of T' over pressure and the pressure and temperature derivatives of C_p^c . The pressure derivative gives $(\partial C_p^c/\partial P)_T = -T_g V_g \Delta \alpha_p^2/k_B$, where V_g is the molecular volume of the glass. The difference of the isobaric expansivities of the liquid and glass, $\Delta \alpha_p$, is in the range $\approx 5 \times 10^{-4} \text{ K}^{-1}$ (Refs. 44 and 120) allowing one to neglect the pressure derivative of C_p^c . One then gets

$$\frac{dT_g}{dP} = \frac{T_g}{T'} \frac{\partial T'}{\partial P} [1 - T'(\partial C_p^c/\partial T)_P]^{-1}. \quad (69)$$

Equation (69) should be compared to what follows from the Adam–Gibbs scaling¹⁶

$$dT_g/dP = T_g V_g \Delta \alpha_p / (S_c + C_p^c). \quad (70)$$

Most data, available for strong/intermediate liquids,^{44,45,124} indicate that Eq. (70) adequately describes the experiment. Since $\partial T_0/\partial P > 0$ (Refs. 123, 124, and 131), one can expect from Eq. (65) that $\partial T'/\partial P > 0$. The actual numbers for this derivative can be obtained from T, P relaxation data.^{120–125,132} The results of these calculation are given in Table III. The relaxation times were fitted to Eq. (61) at ambient pressure with D and T' considered as fitting parameters and experimental $C_p^{\text{ex}}(T)$ and ambient pressure. The parameter D was then kept constant at elevated pressures and $\partial T'/\partial P$ was evaluated from the fit. The results of these calculations are in reasonable agreement with reported dT_g/dP and reproduce the drop of this derivative in going from fragile to intermediate glass formers (Table III).

IV. DISCUSSION

The model developed here describes the thermodynamic properties of glass formers in terms of statistics of excitations from a single-energy state of the ideal glass to a Gaussian manifold of configurationally unjammed states with higher energy and entropy. The model suggests that the thermodynamic signatures of fragile liquids, in particular a sharply increasing configurational heat capacity close to the glass transition, can be identified with the existence of a thermodynamic phase transition [“LL line” in Fig. 14(a)], usually hidden below the glass transition temperature.^{12,82,134} The strong/fragile behavior is distinguished within the model by two parameters, the trapping energy parameter λ and the entropy gain for a single configurational excitation s_0 , the ratio of them equal to the experimental Kauzmann tempera-

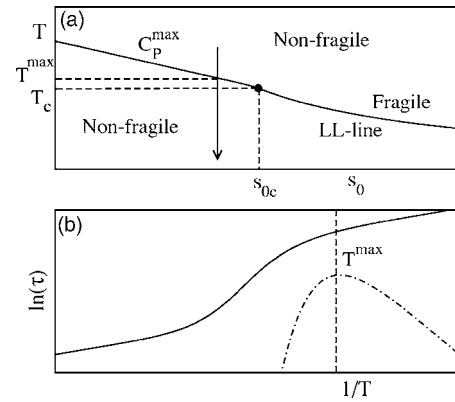


FIG. 14. The liquid-liquid coexistence line (LL line) and the line of maximum heat capacity (Widom line) (Ref. 133) in the (T, s_0) parameters plane (a). Thermodynamic fragile behavior is limited by the critical point (T_c, s_{0c}) [Eq. (37)]. The vertical arrow shows the cooling path along which the relaxation time is calculated using Eq. (61) (b). T^{max} denotes the temperature at which the of heat capacity [dash-dotted line in (b)] passes through a maximum, $C_p^{\text{max}} = C_p(T^{\text{max}})$. All the plots have been generated at constant ϵ_0, λ , and z .

ture [Eq. (38)]. Both parameters significantly decrease when going from fragile to intermediate/strong liquids, with the parameter λ showing the most significant change (Table II). Fragile liquids are therefore characterized by a broad range of configurationally excited states, whereas the energy distribution for intermediate/strong liquids is very narrow (Fig. 1). Because of low values of either λ or s_0 (or both of them) strong/intermediate liquids fall in the range of temperatures and excitation entropies [$T > T_c, s_0 < s_{0c}$, Eq. (37)] not allowing a first-order transition.

The critical point (T_c, s_{0c}) , separating fragile from non-fragile liquids [Fig. 14(a)], makes the descent into the energy landscape qualitatively different for them. The average basin energy of nonfragile liquids first starts to drop from the high-energy plateau according to the $1/T$ law and then inflects into an exponential decay. The distribution of basin energies is narrow, and its maximum shifts to lower energies with cooling [Figs. 15(a) and 15(b)]. This behavior, often observed in simulations of binary LJ liquids,^{30,33,68,96} is well reproduced by the present model which places these fluids into the strong/intermediate category. As an example, we show in Fig. 16 the fit of the IG model to Sastry’s data on binary LJ mixture (BLJM).^{28,135} The calculations were done

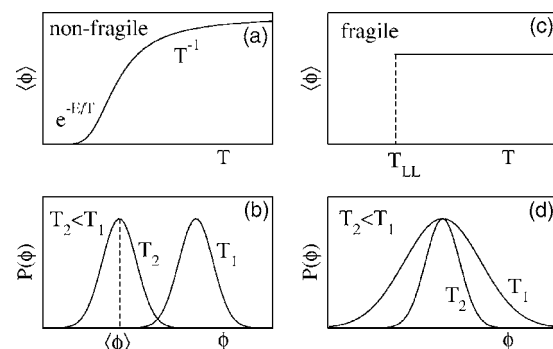


FIG. 15. Illustration of the temperature behavior of the average basin energy $\langle \phi \rangle$ and the distribution of basin energies $P(\phi)$ in nonfragile and fragile liquids.

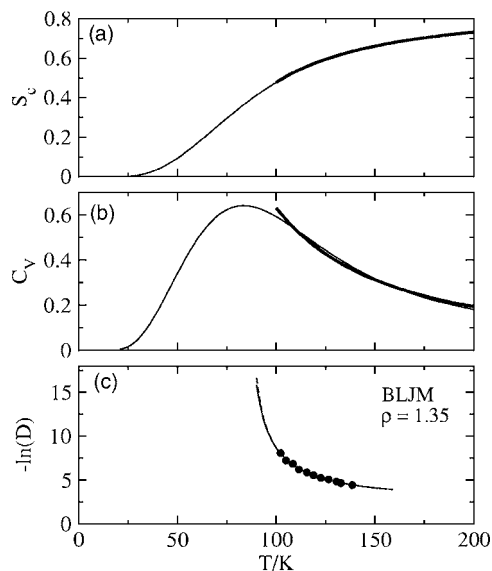


FIG. 16. Configurational entropy (a), configurational (constant-volume) heat capacity (b), and diffusion coefficient (c) of the 80(A):20(B) BLJM liquid at $\rho\sigma_{AA}^3=1.35$, where σ_{AA} is the LJ diameter of the component with higher concentration. The thick solid lines are the results of simulations from Ref. 28 arbitrarily limited to $T > 100$ K. The diffusion coefficients from Ref. 135 [circles, (c)] are fitted to Eq. (61) (solid line) and to the VFT relation (dashed line). The two fits are almost indistinguishable on the scale of the plot. The fitting to 1G model [Eqs. (28), (31), and (61)] results in the following fitting parameters: $\epsilon_0=219$ K, $\lambda=71$ K, $s_0^c=0.32$, $T'=92.8$ K, and $D=3.1$. The thermodynamic Kauzmann temperature T_K is zero when calculated in the 1G model [the thin lines in (a) and (b)].

for the highest density studied in simulations at which the BLJM liquid is most fragile. Equations (28) and (31) were used, respectively, for the configurational entropy and heat capacity, while Eq. (61) was applied to the simulated diffusivity. The excitation energy ($\epsilon_0=219$ K) and the trapping energy ($\lambda=71$ K) obtained from the fit produce the following critical parameters: $T_c=35.5$ K and $s_{0c}=4.2$ (accidentally, T_c is close to T_K^{exp}). On the other hand, the excitation entropy from the fit, $s_0^c=0.32$, and the temperature range $T > T_c$ together put the BLJM liquid into the category of intermediate fragility. With such low excitation entropy, the population of the excited state is close to 0.5 at high temperatures. From Eq. (28) one then gets ($z=1$) $S_0=s_0^c/2 + \ln(2) \approx 0.85$. The same number, 0.85, is reported by Sastry for the top of the enumeration function s_{max}^c .²⁸

The behavior of fragile liquids is quite different. The configurationally excited state is almost entirely populated ($x \approx 1$) in the entire range of experimentally accessible temperatures down to the glass transition. The average basin energy is almost temperature independent and the only effect of lowering the temperature on the distribution of basin energies is its narrowing according to the fluctuation-dissipation theorem [Figs. 15(c) and 15(d)]. The invariant population of the configurationally excited states is abruptly terminated at the equilibrium first-order transition or (on supercooling) at spinodal instability at which point it drops to a low value representative of an entropy-poor, low-temperature phase as experimentally confirmed for TPP.¹³⁶

The fit of the model to experimental excess heat capacities and entropies of molecular glass formers (Table II) has

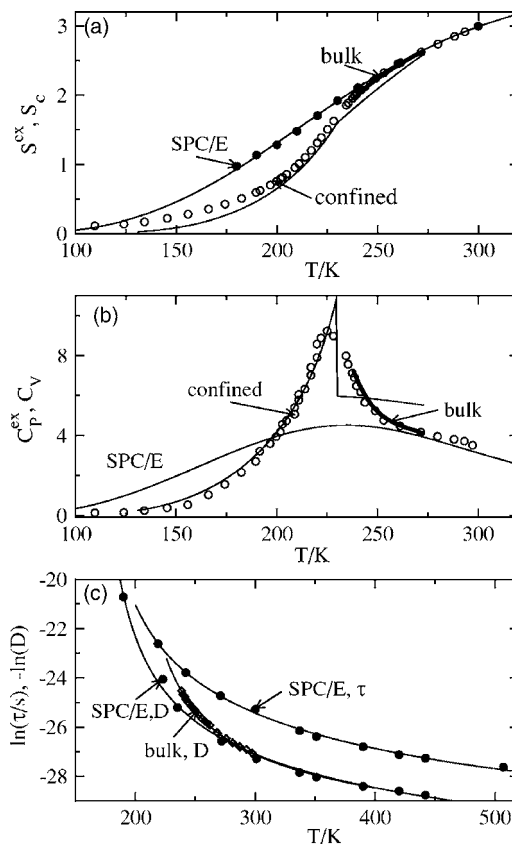


FIG. 17. (a) Excess entropy for bulk laboratory water (bulk), nanoconfined water (confined), and configurational entropy for SPC/E water (SPC/E). The thick line and open points refer to bulk (Ref. 139) and nanoconfined experiments, respectively. The closed points refer to constant-volume simulations (Ref. 137). (b) Experimental excess heat capacity for bulk (thick line) (Ref. 139) and hard nanoconfined (Ref. 140) (open points) water. The thin lines in (a) and (b) are fits to the thermodynamic 1G model [Eqs. (27) and (29)]. The configurational heat capacity of SPC/E water in (b) is calculated from the fit of the configurational entropy in (a). (c) Simulation (constant-volume) results for the Debye relaxation time (SPC/E, τ) and diffusivity (SPC/E, D) of SPC/E water (Ref. 141). Diamonds show experimental diffusivity of laboratory water (Ref. 142). The solid lines are fits to Eq. (61) with the configurational heat capacity obtained by numerical differentiation of S_c for SPC/E water (see Table IV for the fitting parameters). The diffusivity curves have been arbitrarily shifted to fit to the scale of the plot. For all three panels, the closed points refer to simulations and open points are used to indicate the laboratory experiment.

pushed the liquid-liquid phase transition below the glass transition. For some substances,^{3,133,137,138} the thermodynamic liquid-liquid transition can be found above the glass transition. As an example of this situation, the 1G model is applied to excess entropy and heat capacity of laboratory water.^{139,140} The thick lines in Figs. 17(a) and 17(b) show the results of measurements on bulk samples,¹³⁹ while open circles refer to samples confined in 3 nm pores of silica gel.¹⁴⁰ The two sets of data coincide at high temperatures. Because of the limited temperature range of the bulk water data, the fit to the thermodynamic 1G model is done for nanoconfined water (Table IV). The 1G model predicts a weak first-order phase transition at $T_{LL}=229$ K ($P=1$ atm). This number is very close to previous estimates for the temperature of crossing the “Widom line” at which the heat capacity gets a maximum¹³⁷ and more recent measurements placing this point at 223 K.¹⁴⁴ After the kink at T_{LL} , the entropy slowly decays to zero at $T_K \rightarrow 0$.

TABLE IV. Fit of the 1G model to excess thermodynamics (Refs. 139 and 140) and diffusivity (Ref. 142) of laboratory water and to configurational entropy, diffusivity, and Debye relaxation time of SPC/E water from constant-volume simulations (Refs. 137, 141, and 143) ($\rho=1.0\text{ g/cm}^3$). The heat capacity and excess entropy of nanoconfined water (Ref. 140) are used for the thermodynamic fitting. The energy parameters are in kelvin, D and z are dimensionless.

Liquid	ϵ_0	λ	s_0	s_{0c}	z	D	T'	$\log(\tau_0/s)$
Bulk/confined water	1298	649	2.8	2.0	3.0	66 ^a	19	
SPC/E water	751	251	1.3 ^b	4.0	3.0	282 ^c 193 ^d	5.7 7.6	-13.4

^aFrom fitting the diffusivity of laboratory water according to Price *et al.* (Ref. 142).

^bConfigurational component s_0^c of the excitation entropy.

^cFrom fitting the Debye relaxation time.

^dFrom fitting the diffusivity.

The behavior of excess thermodynamic parameters of the laboratory water is compared to configurational parameters of SPC/E water obtained from constant-volume simulations of Starr *et al.*^{137,143} The fit of Eqs. (28) and (29) to the configurational entropy of SPC/E water [Fig. 17(a) and Table IV] yields a low excitation entropy $s_0^c=1.3$, below the critical value of $s_{0c}=4.0$ [Eq. (37)]. The heat capacity curve then shows a broad precritical peak reminiscent of, but broader than, the heat capacity of nanoconfined water [Fig. 17(b)]. As in the case of the BLJM liquid, the excited state population, characterizing the configurational manifold, is slightly above 0.5 at high temperatures resulting in the plateau of the configurational entropy at ($z=3$) $S_0 \approx z[s_0^c/2 + \ln(2)] \approx 4$. This number is close to the estimate for the top of the enumeration function given by Sciortino,⁴² $S_0 \approx 3.7$ at $P \approx 0$.

The comparison of fits to laboratory and simulation data shows that the configurational part of the excitation entropy s_0^c makes about 46% of s_0 for SPC/E water and only about 30% for *o*-terphenyl (Fig. 6). These comparable fractions of configurational components suggest that it is the change in the vibrational density of states (around the boson peak at $\approx 30\text{ cm}^{-1}$) caused by configurational excitations that is primarily responsible for the fragile behavior of glass formers.³⁷

The configurational entropy from simulations can next be used to fit the relaxation times by applying Eq. (61). This procedure is straightforward for the Debye relaxation time and diffusivity obtained from constant-volume simulations¹⁴¹ at the same conditions as the data shown in Fig. 17(a) (see Table IV for the fitting parameters). The application to laboratory data is less obvious because of possible differences between configurational heat capacities at constant volume and constant pressure. Nevertheless, diffusivity of laboratory water¹⁴² can be fitted to Eq. (61), although with the fitting parameters (Table IV) requiring more fragile behavior [cf. diamonds to circles in Fig. 17(c)].

Equation (61) is the central result of our modeling of relaxation. It is also consistent with the empirically documented accord between the VFT and Kauzmann temperatures (Fig. 13). The model combines the thermodynamics of configurational excitations with the notion that assembling excited units in clusters is required for activated relaxation.¹⁴⁵ The thermodynamics of glass formers is thus determined by the statistics of excitations, while dynamics probe more rare events of clustering of excitations. One of the signatures of thermodynamic driving force behind relax-

ation is the realization of a dynamic fragile-to-strong transition close to the point where the heat capacity in the denominator of Eq. (61) reaches its maximum, C_P^{\max} . This subcritical maximum is indeed predicted by the thermodynamic 1G model in the vicinity of the critical point (T_c, s_{0c}) [Fig. 14(a)]. When the cooling path goes close to the critical point, the fragile non-Arrhenius dynamics changes to strong Arrhenius dynamics after passing the line of the heat capacity maximum [Widom line,¹³³ Fig. 14(b)]. A similar behavior has recently been observed for nanoconfined water.^{144,146}

Experimental evidence supports a link between the viscosity and configurational thermodynamics^{28,33,34,147} but this does not necessarily mean that activated events are driven by the entropy. Equation (61) still connects the relaxation time to configurational entropy [see Eq. (68)], but is based on the standard arguments of activated kinetics in terms of excess kinetic energy accumulated at a “mobile unit.” The model thus puts focus on the kinetic energy and its fluctuations as the main driving force of liquid relaxation.¹⁹ This notion brings relaxation of supercooled liquid in general accord with approaches developed to describe activated events in chemistry where accumulation of sufficient kinetic energy along a reaction coordinate, and not the entropy, is viewed as the general mechanism behind activated transitions. Since relaxation is understood in terms of clusters of excitations, the model can potentially bridge to more macroscopic arguments of elastic theories considering a region of shear displacements shoving the environment from a relaxing unit.⁴⁷

The present model does not anticipate a divergent length scale and also avoids the need to consider the mosaic interface energies of Ref. 20, which recent simulations have failed to support.¹⁰¹ (This failure might be related to the fractal nature of reconfiguring regions near the crossover temperature.¹⁴⁸) It remains to be seen whether the formalism of configurational excitations,^{53,55-57,149} “dressed” with the relevant excitation thermodynamics, provides a sufficient basis for the theoretical modeling of supercooled liquids. While the model yields a set of simple equations for some basic properties commonly reported for glass formers [e.g., Eqs. (32), (38), (37), and (61)], it should be recognized that the mean-field character of the model may push it too much into a strong first-order type of thermodynamic transition. Some “softening” of the model including fluctuations around the

mean field would result in greater flexibility, but this would only come at the expense of an increase in the number of parameters.

ACKNOWLEDGMENTS

The authors are grateful to Ranko Richert for the help with dielectric relaxation data and to Srikanth Sastry for useful discussions. This work was supported by the NSF through the Grant Nos. CHE-0616646 (D.V.M.) and DMR-0082535 (C.A.A.). C.A.A. thanks Francesco Sciortino for a number of illuminating discussions. They also thank Karl Freed and Peter Wolynes for critical comments on the manuscript.

- ¹K. L. Ngai, *J. Non-Cryst. Solids* **275**, 7 (2000).
- ²C. A. Angell, *Science* **267**, 1924 (1995).
- ³C. A. Angell, K. L. Ngai, G. B. McKenna, and S. W. Martin, *J. Appl. Phys.* **88**, 3113 (2000).
- ⁴W. Götze, in *Liquids, Freezing and Glass Transition*, edited by J. P. Hansen, D. Levesque, and J. Zinn-Justin (Elsevier, Amsterdam, 1991), Vol. 1, p. 287.
- ⁵P. G. Debenedetti and F. H. Stillinger, *Nature (London)* **410**, 259 (2001).
- ⁶M. Goldstein, *J. Chem. Phys.* **51**, 3728 (1969).
- ⁷B. Doliwa and A. Heuer, *Phys. Rev. E* **67**, 031506 (2003).
- ⁸R. A. Denny, D. R. Reichman, and J.-P. Bouchaud, *Phys. Rev. Lett.* **90**, 025503 (2003).
- ⁹A. Heuer, B. Doliwa, and A. Saksengwitt, *Phys. Rev. E* **72**, 021503 (2005).
- ¹⁰V. N. Novikov and A. P. Sokolov, *Phys. Rev. E* **67**, 031507 (2003).
- ¹¹G. Adam and J. H. Gibbs, *J. Chem. Phys.* **43**, 139 (1965).
- ¹²J. H. Gibbs and E. A. D. Marzio, *J. Chem. Phys.* **28**, 373 (1958).
- ¹³E. A. D. Marsio and A. J. M. Yang, *J. Res. Natl. Inst. Stand. Technol.* **102**, 135 (1997).
- ¹⁴J. Dudowicz, K. F. Freed, and J. F. Douglas, *Adv. Chem. Phys.* (in press).
- ¹⁵W. Kauzmann, *Chem. Rev. (Washington, D.C.)* **43**, 219 (1948).
- ¹⁶P. G. Debenedetti, *Metastable Liquids: Concepts and Principles* (Princeton University Press, Princeton, NJ, 1996).
- ¹⁷M. H. Cohen and D. Turnbull, *J. Chem. Phys.* **31**, 1164 (1959).
- ¹⁸M. H. Cohen and G. Grest, *Adv. Chem. Phys.* **48**, 370 (1981).
- ¹⁹M. L. Ferrer, C. Lawrence, B. G. Demirjian, and D. Kivelson, *J. Chem. Phys.* **109**, 8010 (1998).
- ²⁰X. Xia and P. G. Wolynes, *Proc. Natl. Acad. Sci. U.S.A.* **97**, 2990 (2000).
- ²¹X. Xia and P. G. Wolynes, *J. Phys. Chem. B* **105**, 6570 (2001).
- ²²V. Lubchenko and P. G. Wolynes, *J. Chem. Phys.* **121**, 2852 (2004).
- ²³V. Lubchenko and P. G. Wolynes, *cond-mat/0506708*.
- ²⁴J.-P. Bouchaud and G. Biroli, *J. Chem. Phys.* **121**, 7347 (2004).
- ²⁵T. R. Kirkpatrick, D. Thirumalai, and P. G. Wolynes, *Phys. Rev. A* **40**, 1045 (1989).
- ²⁶C. A. Angell, *J. Non-Cryst. Solids* **131-133**, 13 (1991).
- ²⁷R. Richert and A. C. Angell, *J. Chem. Phys.* **108**, 9016 (1998).
- ²⁸S. Sastry, *Nature (London)* **409**, 164 (2001).
- ²⁹I. Saika-Voivod, P. H. Poole, and F. Sciortino, *Nature (London)* **412**, 514 (2001).
- ³⁰S. Mossa, E. L. Nave, H. E. Stanley, C. Donati, F. Sciortino, and P. Tartaglia, *Phys. Rev. E* **65**, 041205 (2002).
- ³¹N. Giovambattista, S. V. Buldyrev, F. W. Starr, and H. E. Stanley, *Phys. Rev. Lett.* **90**, 085506 (2003).
- ³²I. Saika-Voivod, F. Sciortino, and P. H. Poole, *Phys. Rev. E* **69**, 041503 (2004).
- ³³Y. Gebremichael, M. Vogel, M. N. J. Bergroth, F. W. Starr, and S. C. Glotzer, *J. Phys. Chem. B* **109**, 15068 (2005).
- ³⁴I. Saika-Voivod, F. Sciortino, and P. H. Poole, *cond-mat/0309481*.
- ³⁵M. J. Goldstein, *J. Chem. Phys.* **64**, 4767 (1976).
- ³⁶G. P. Johari, *J. Chem. Phys.* **112**, 7518 (2000).
- ³⁷C. A. Angell and S. Borick, *J. Non-Cryst. Solids* **307-310**, 393 (2002).
- ³⁸R. J. Speedy, *J. Chem. Phys.* **116**, 4228 (2002).
- ³⁹G. P. Johari, *J. Phys. Chem. B* **107**, 5048 (2003).
- ⁴⁰Y. Privalko, *J. Phys. Chem.* **84**, 3307 (1980).
- ⁴¹E. La Nave, S. Mossa, and F. Sciortino, *Phys. Rev. Lett.* **88**, 225701 (2002).
- ⁴²F. Sciortino, *J. Stat. Mech.: Theory Exp.* 2005, P05015.
- ⁴³C. A. Angell, *J. Res. Natl. Inst. Stand. Technol.* **102**, 171 (1997).
- ⁴⁴M. Goldstein, *J. Chem. Phys.* **39**, 3369 (1963).
- ⁴⁵C. A. Angell and W. Sichina, *Ann. N.Y. Acad. Sci.* **279**, 53 (1976).
- ⁴⁶A. Barkatt and C. A. Angell, *J. Chem. Phys.* **70**, 901 (1979).
- ⁴⁷J. C. Dyre, *Rev. Mod. Phys.* **78**, 953 (2006).
- ⁴⁸S. A. Brawer, *J. Chem. Phys.* **81**, 954 (1984).
- ⁴⁹C. Monthus, and J.-P. Bouchaud, *J. Phys. A* **29**, 3847 (1996).
- ⁵⁰H. Bässler, *Phys. Rev. Lett.* **58**, 767 (1987).
- ⁵¹V. I. Arkhipov and H. Bässler, *J. Phys. Chem.* **98**, 662 (1994).
- ⁵²J. C. Dyre, *Phys. Rev. B* **51**, 12276 (1995).
- ⁵³C. A. Angell and K. J. Rao, *J. Chem. Phys.* **57**, 470 (1972).
- ⁵⁴C. T. Moynihan and C. A. Angell, *J. Non-Cryst. Solids* **274**, 131 (2000).
- ⁵⁵J. P. Garrahan and D. Chandler, *Proc. Natl. Acad. Sci. U.S.A.* **100**, 9710 (2003).
- ⁵⁶M. Goldstein, *Symp. Faraday Soc.* **6**, 7 (1972).
- ⁵⁷D. V. Matyushov and C. A. Angell, *J. Chem. Phys.* **123**, 034506 (2005).
- ⁵⁸F. H. Stillinger, *J. Chem. Phys.* **88**, 7818 (1988).
- ⁵⁹J. D. Bryngelson and P. G. Wolynes, *Proc. Natl. Acad. Sci. U.S.A.* **84**, 7524 (1987).
- ⁶⁰K. F. Freed, *J. Chem. Phys.* **119**, 5730 (2003).
- ⁶¹A. A. Angell, Y. Yue, L.-M. Wang, J. R. D. Copley, S. Borick, and S. Mossa, *J. Phys.: Condens. Matter* **15**, S1051 (2003).
- ⁶²L. D. Landau and E. M. Lifshits, *Statistical Physics* (Pergamon, New York, 1980).
- ⁶³J. P. Hansen and I. R. McDonald, *Theory of Simple Liquids* (Academic, New York, 2003).
- ⁶⁴R. Richert and H. Bässler, *J. Phys.: Condens. Matter* **2**, 2273 (1990).
- ⁶⁵B. Derrida, *Phys. Rev. B* **24**, 2613 (1981).
- ⁶⁶K. H. Fischer and J. A. Hertz, *Spin Glasses* (Cambridge University Press, Cambridge, 1999).
- ⁶⁷F. H. Stillinger and T. A. Weber, *Phys. Rev. A* **25**, 978 (1982).
- ⁶⁸S. Sastry, P. G. Debenedetti, and F. H. Stillinger, *Nature (London)* **393**, 554 (1998).
- ⁶⁹A. Heuer and S. Büchner, *J. Phys.: Condens. Matter* **12**, 6535 (2000).
- ⁷⁰D. V. Matyushov, *cond-mat/0701056*.
- ⁷¹A. Saksengwitt, J. Reinisch, and A. Heuer, *Phys. Rev. Lett.* **93**, 235701 (2004).
- ⁷²J. D. Bryngelson and P. G. Wolynes, *J. Phys. Chem.* **93**, 6902 (1989).
- ⁷³S. Strässler and C. Kittel, *Phys. Rev.* **139**, A758 (1965).
- ⁷⁴E. Rapoport, *J. Chem. Phys.* **46**, 2891 (1967).
- ⁷⁵L. I. Aptekar, *Sov. Phys. Dokl.* **24**, 993 (1979).
- ⁷⁶E. G. Ponyatovsky, *J. Phys.: Condens. Matter* **15**, 6123 (2003).
- ⁷⁷A. V. Granato, *Phys. Rev. Lett.* **68**, 974 (1992).
- ⁷⁸C. A. Angell and C. T. Moynihan, *Metall. Mater. Trans. B* **31B**, 587 (2000).
- ⁷⁹P. G. Wolynes, *J. Res. Natl. Inst. Stand. Technol.* **102**, 187 (1997).
- ⁸⁰J. M. Ziman, *Models of Disorder* (Cambridge University Press, Cambridge, 1979).
- ⁸¹Y. Singh, J. P. Stoessel, and P. G. Wolynes, *Phys. Rev. Lett.* **54**, 1059 (1985).
- ⁸²W. Klein, H. Gould, R. A. Ramos, I. Clejan, and A. I. Mel'cuk, *Physica A* **205**, 738 (1994).
- ⁸³A. I. Mel'cuk, R. A. Ramos, H. Gould, W. Klein, and R. D. Mountain, *Phys. Rev. Lett.* **75**, 2522 (1995).
- ⁸⁴R. V. Chamberlin, *Nature (London)* **408**, 337 (2000).
- ⁸⁵B. Wunderlich, *J. Phys. Chem.* **64**, 1052 (1960).
- ⁸⁶L.-M. Wang, V. Velikov, and C. A. Angell, *J. Chem. Phys.* **117**, 10184 (2002).
- ⁸⁷J. D. Stevenson and P. G. Wolynes, *J. Phys. Chem. B* **109**, 15093 (2005).
- ⁸⁸K. Takeda, O. Yamamuro, I. Tsukushi, T. Matsuo, and H. Suga, *J. Mol. Struct.* **479**, 227 (1999).
- ⁸⁹A. Döss, G. Hinze, B. Schiener, J. Hemberger, and R. Böhmer, *J. Chem. Phys.* **107**, 1740 (1997).
- ⁹⁰N. Menon, K. P. O'Brien, P. K. Dixon, L. Wu, and S. R. Nagel, *J. Non-Cryst. Solids* **141**, 61 (1992).
- ⁹¹P. K. Ghorai and D. V. Matyushov, *J. Phys. Chem. A* **110**, 8857 (2006).
- ⁹²N. Hirai and H. Eyring, *J. Appl. Phys.* **29**, 810 (1958).
- ⁹³L.-M. Wang and C. A. Angell, *Nature (London)* **410**, 663 (2001).
- ⁹⁴L.-M. Wang, C. A. Angell, and R. Richert, *J. Chem. Phys.* **125**, 074505 (2006).
- ⁹⁵D. Chandler and J. P. Garrahan, *J. Chem. Phys.* **123**, 044511 (2005).
- ⁹⁶S. Büchner and A. Heuer, *Phys. Rev. E* **60**, 6507 (1999).
- ⁹⁷A. J. Moreno, I. Saika-Voivod, E. Zaccarelli, E. L. Nave, S. V. Buldyrev,

- P. Tartaglia, and F. Sciortino, *J. Chem. Phys.* **124**, 204509 (2006).
- ⁹⁸ J. Gerardin, S. Mohanty, and U. Mohanty, *J. Chem. Phys.* **119**, 4473 (2003).
- ⁹⁹ A. Saksangwijit and A. Heuer, *Phys. Rev. E* **73**, 061503 (2006).
- ¹⁰⁰ R. G. Palmer, D. L. Stein, E. Abrahams, and P. W. Anderson, *Phys. Rev. Lett.* **53**, 958 (1984).
- ¹⁰¹ A. Cavagna, T. S. Grigera, and P. Verrocchio, *cond-mat/0607817* (2006).
- ¹⁰² J. S. Langer, *Phys. Rev. Lett.* **97**, 115704 (2006).
- ¹⁰³ M. D. Ediger, *Annu. Rev. Phys. Chem.* **51**, 99 (2000).
- ¹⁰⁴ R. Richert, *J. Phys.: Condens. Matter* **14**, R703 (2002).
- ¹⁰⁵ C. Donati, J. F. Douglas, W. Kob, S. J. Plimpton, P. H. Poole, and S. C. Glotzer, *Phys. Rev. Lett.* **80**, 2338 (1998).
- ¹⁰⁶ A. Widmer-Cooper, P. Harrowell, and H. Fynewever, *Phys. Rev. Lett.* **93**, 135701 (2004).
- ¹⁰⁷ T. A. Vilgis, in *Disorder Effects on Relaxational Processes*, edited by R. Richert and A. Blumen (Springer, Berlin, 1994), p. 153.
- ¹⁰⁸ F. Ritort and P. Sollich, *Adv. Phys.* **52**, 219 (2003).
- ¹⁰⁹ J. J. Brey and A. Prados, *Phys. Rev. E* **63**, 021108 (2001).
- ¹¹⁰ E. Abrahams, *Phys. Rev. E* **71**, 051901 (2005).
- ¹¹¹ R. Böhmer and C. A. Angell, in *Disorder Effects on Relaxational Processes*, edited by R. Richert and A. Blumen (Springer, Berlin, 1994).
- ¹¹² J. Frenkel, *Kinetic Theory of Liquids* (Dover, New York, 1955).
- ¹¹³ D. G. Cahill and R. O. Pohl, *Annu. Rev. Phys. Chem.* **39**, 93 (1988).
- ¹¹⁴ P. Sheng, M. Zhou, and Z.-Q. Zhang, *Phys. Rev. Lett.* **72**, 234 (1994).
- ¹¹⁵ W. Schirmacher, G. Diezemann, and C. Ganter, *Phys. Rev. Lett.* **81**, 136 (1998).
- ¹¹⁶ W. Forst, *Unimolecular Reactions. A Concise Introduction* (Cambridge University Press, Cambridge, 2003).
- ¹¹⁷ T. A. Litovitz, *J. Chem. Phys.* **20**, 1088 (1952).
- ¹¹⁸ V. N. Novikov, Y. Ding, and A. P. Sokolov, *Phys. Rev. E* **71**, 061501 (2005).
- ¹¹⁹ E. A. Jagla, *J. Phys.: Condens. Matter* **11**, 10251 (1999).
- ¹²⁰ T. Atake and C. A. Angell, *J. Phys. Chem.* **83**, 3218 (1979).
- ¹²¹ R. Casalini, M. Paluch, and C. M. Roland, *J. Phys. Chem. A* **107**, 2369 (2003).
- ¹²² C. M. Roland, S. Hensel-Bielowka, M. Paluch, and R. Casalini, *Rep. Prog. Phys.* **68**, 1405 (2005).
- ¹²³ R. L. Cook, J. H. E. King, C. A. Herbst, and D. R. Herschbach, *J. Chem. Phys.* **100**, 5178 (1994).
- ¹²⁴ S. Takahara, O. Yamamuro, and H. Suga, *J. Non-Cryst. Solids* **171**, 259 (1994).
- ¹²⁵ A. Gilchrist, J. E. Earley, and R. H. Cole, *J. Chem. Phys.* **26**, 196 (1957).
- ¹²⁶ E. Donth, *J. Non-Cryst. Solids* **131-133**, 204 (1991).
- ¹²⁷ L. Berthier, G. Biroli, J.-P. Bouchaud, L. Cipelletti, D. E. Marsi, D. L'Hôte, F. Ladieu, and M. Pierno, *Science* **310**, 1797 (2005).
- ¹²⁸ J. D. Stevenson and P. G. Wolynes, *cond-mat/0609677*.
- ¹²⁹ G. Ruocco, F. Sciortino, F. Zamponi, C. D. Michele, and T. Scopigno, *J. Chem. Phys.* **120**, 10666 (2004).
- ¹³⁰ E. Donth, *The Glass Transition: Relaxation Dynamics in Liquids and Disordered Materials* (Springer, Berlin, 2001).
- ¹³¹ R. Casalini, S. Capaccioli, M. Lucchesi, and P. A. Rolla, *Phys. Rev. E* **63**, 031207 (2001).
- ¹³² C. Dreyfus, A. Aouadi, M. Matos-Lopes, W. Steffen, A. Patkowski, and R. M. Pick, *Phys. Rev. E* **68**, 011204 (2003).
- ¹³³ L. Xu, P. Kumar, S. V. Buldyrev, S.-H. Chen, P. H. Poole, F. Sciortino, and H. E. Stanley, *Proc. Natl. Acad. Sci. U.S.A.* **102**, 16558 (2005).
- ¹³⁴ J. S. Sethna, J. D. Shore, and M. Huang, *Phys. Rev. B* **44**, 4943 (1991).
- ¹³⁵ S. Sastry, *Phys. Rev. Lett.* **85**, 590 (2000).
- ¹³⁶ R. Kurita and H. Tanaka, *Science* **306**, 845 (2004).
- ¹³⁷ F. W. Starr, C. A. Angell, and H. E. Stanley, *Physica A* **323**, 51 (2003).
- ¹³⁸ H. Tanaka, *Phys. Rev. E* **62**, 6968 (2000).
- ¹³⁹ C. A. Angell, in *Water and Steam*, edited by J. Staub and K. Scheffler (Pergamon, Oxford, 1980), p. 233.
- ¹⁴⁰ S. Maruyama, K. Wakabayashi, and M. Oguni, *AIP Conf. Proc.* **708**, 675 (2004).
- ¹⁴¹ P. K. Ghorai and D. V. Matyushov, *J. Phys. Chem. B* **110**, 1866 (2006b).
- ¹⁴² W. S. Price, H. Ide, and Y. Arata, *J. Phys. Chem. A* **103**, 448 (1999).
- ¹⁴³ F. W. Starr, S. Sastry, E. L. Nave, A. Scala, H. E. Stanley, and F. Sciortino, *Phys. Rev. E* **63**, 041201 (2001).
- ¹⁴⁴ F. Mallamace, M. Broccio, C. Corsaro, A. Faraone, U. Wanderlingh, L. Liu, C.-Y. Mou, and S. H. Chen, *J. Chem. Phys.* **124**, 161102 (2006).
- ¹⁴⁵ J. F. Douglas, J. Dudowicz, and K. F. Freed, *J. Chem. Phys.* **125**, 144907 (2006).
- ¹⁴⁶ L. Liu, S.-H. Chen, A. Faraone, C.-W. Yen, and C.-Y. Mou, *Phys. Rev. Lett.* **95**, 117802 (2005).
- ¹⁴⁷ G. W. Scherer, *J. Non-Cryst. Solids* **123**, 75 (1990).
- ¹⁴⁸ J. D. Stevenson, J. Schmalian, and P. G. Wolynes, *Nat. Phys.* **2**, 268 (2006).
- ¹⁴⁹ H. Tanaka, *J. Phys.: Condens. Matter* **15**, L491 (2003).